5-2022

Tribological Characterization of Nickel-Based Cold Spray Coatings for Aerospace and Industrial Manufacturing

Albert Alejandro
The University of Texas Rio Grande Valley

TRIBOLOGICAL CHARACTERIZATION OF NICKEL-BASED COLD SPRAY COATINGS FOR AEROSPACE AND INDUSTRIAL MANUFACTURING

A Thesis

by

ALBERT ALEJANDRO

Submitted in Partial Fulfillment of the

Requirements for the Degree of

MASTER OF SCIENCE IN ENGINEERING

Major Subject: Mechanical Engineering

The University of Texas Rio Grande Valley

May 2022

TRIBOLOGICAL CHARACTERIZATION OF NICKEL-BASED COLD SPRAY COATINGS FOR AEROSPACE AND INDUSTRIAL MANUFACTURING

A Thesis
by
ALBERT ALEJANDRO

COMMITTEE MEMBERS

Dr. Javier A. Ortega
Chair of Committee

Dr. Jianzhi Li
Committee Member

Dr. Horacio Vasquez
Committee Member

May 2022

ABSTRACT

Alejandro, Albert, Tribological Characterization of Nickel-Based Cold Spray Coatings for Aerospace and Industrial Manufacturing. Master of Science Mechanical Engineering (MSE), May, 2022, 92 pp., 4 tables, 51 figures, references, 39 titles.

Cold Spray Additive Manufacturing (CSAM) is a sub-category of thermal spray technology where a metal powder is accelerated in a gas stream toward a metal substrate at high velocities, producing a metallurgical bond with the metal substrate on impact. The present study investigates the effect of Al_2O_3 additions on the tribological properties of nickel-based cold spray coatings deposited on aluminum 6061 for aerospace and industrial manufacturing. The tribological performance of the nickel-based cold spray coatings with and without Al_2O_3 additions was evaluated using an abrasive wear test based on the ball-crater technique. In addition, the wear and friction characteristics of the CSAM coatings were evaluated with a pin-on-disk tribometer. It was found that the addition of Al_2O_3 particles did not provide any improvement in the tribological properties of the coating. However, the addition of alumina particles was highly effective in decreasing porosity in the coating.

DEDICATION

I dedicate this thesis to my family members who have supported me and allowed me to get this far in my education. I would like to thank my mother, Hilda Alejandro Vallejo, who has been supportive of me furthering my education and has instilled in me a high sense of confidence in myself. I would also like to dedicate this to my father, Alberto Alejandro who has shared his work ethic with me and has taught me to never give up and persevere. I also have done this thesis to set a high standard for my two younger brothers, Kevin, and Justin, who also aspire to become professionals. As the elder brother, I feel a sense of duty to be the best example that I can be and teach them how to succeed as professionals. I would also like to give a special thanks to my Grandparents, José Manuel Vallejo, and Olga Maldonado Vallejo, who have provided me with mental and emotional support and have set a good example for me. They have been the supporting pillar in my personal life and without them I could not have achieved this.

ACKNOWLEDGMENTS

When starting the master's program in engineering, I choose Dr. Javier A. Ortega as my advisor, because of his incredible work ethic, and because I never forgot the unwavering support, he provided me as an undergraduate student. Dr. Ortega has made the seemingly impossible possible and has moved mountains for me to become a professional engineer with knowledge in a wide range of engineering disciplines. I am very fortunate to have had the opportunity to start a new type of research with Dr. Ortega and am proud to have opened the door to future research in this topic at UTRGV. I would also like to thank Dr. Jianzhi Li, who offered his support for this research and has made it possible for me to take part in research in collaboration with TMAC and the Department of Manufacturing and Industrial Engineering. I would like to acknowledge Dr. Horacio Vasquez for his support throughout my path to earn a Master of Science in Mechanical Engineering. A special thanks also goes to Dr. Mataz Alcoutlabi, who was my first instructor at UTRGV and has always believed in me, his words of encouragement to me as an undergraduate student had a great impact on me and gave me the self-confidence in myself to not be afraid to dream about something more. I would also like to acknowledge Dr. Karen Lozano, who spiked my interest in starting my master's degree after lighting the spark of enthusiasm for research in the field of engineering. Without these mentors and role models, I would not be breaking barriers and opening these new doors in my professional career as a mechanical engineer.

TABLE OF CONTENTS

Page

LIST OF TABLES

Page

LIST OF FIGURES

Page

CHAPTER I

INTRODUCTION

1.1 Problem Statement

The use of aluminum alloys as a lightweight structural material for high-volume aerospace/automotive applications is currently a key area of investigation. Although aluminum alloys have acceptable surface properties in certain applications, the wear and corrosion resistance of aluminum alloys is generally poor. Aluminum alloys are widely used in civilian and military fighter aircraft structure, such as the wing box structure, spars, stringers, framework and pressure bulkhead, and fuselage bulkheads. These structures carry high loads and are typically classified as fracture critical components of the aircraft. In addition to the aircraft safety, the fatigue and corrosion damage also involves substantial costs resulting from damage inspections, maintenance, and replacement. Because of the high costs involved in replacing failed components and often the long lead time, aircraft engineers prefer to seek more effective on-site repair solutions instead of replacing the failed part.

Several processes, such as thermal spray and laser cladding, have been developed for aircraft structural repair in past decades. However, those processes commonly involve local melting and solidification of metals, which may introduce oxidation of metals during the

repairing process. Because oxides can act as crack initiators, these impurities in aerospace components must be minimized.

1.2 Purpose Statement

As additive manufacturing is more widely used in industry and researched more in-depth, CSAM (Cold Spray Additive Manufacturing) has emerged as one of the leading thermal spray manufacturing methods. In this coating process, a metal powder is accelerated in a gas stream toward a metal substrate at velocities of 500–1000 m/s, producing a metallurgical bond with the metal substrate on impact. In addition, particle reinforced metal matrix composites (MMCs) are a useful class of material that enables physical properties such as density and thermal or electrical conductivity to be tailored, along with mechanical properties such as strength and wear resistance. MMCs generally comprise a hard reinforcing non-metallic material contained in a ductile, metallic matrix. One such system is Ni and Ni-based alloys, which exhibit high hardiness and corrosion resistance that is reinforced using hard secondary phases to improve their tribological properties. Moreover, it has been reported that cold spraying has great potential in producing MMCs, especially particle reinforced MMCs.

The main purpose of this research project will be to characterize and analyze nickel based CSAM coatings deposited on aluminum substrates and study the effect of hard reinforcing particles (Al_2O_3) on their mechanical and tribological properties. These coatings will be tailored for defense equipment corrosion protection, rapid repair, and restoration applications. The CSAM coatings will be characterized using scanning electron microscopy, and microhardness. The tribological response of the two different surface conditions will be investigated by means of a pin-on-disk wear testing machine and an abrasive wear test based on the ball-crater technique.

CHAPTER II

LITERATURE REVIEW

2.1 Introduction to CSAM

There has been an increase in the use of specialized coatings for metal components such as ball bearings, gears, and other mechanical components which undergo a lot of wear due to friction [1], require better mechanical properties and need protection against corrosion [2]. Cold Spray Additive Manufacturing (CSAM) was first introduced in Russia in the early-mid 1980's by the Russian engineer Anatoli Papyrin and his design team of engineers [3]. This method is a sub-category of the thermal spray family as it has many similar applications and characteristics with other thermal spraying methods, which include wire arc, wire frame and plasma spray methods and many others [4, 5, 6]. What sets this method apart from traditional thermal spray methods, is that it not only relies on the heating element to make sure the particles become semi-melted and coat the substrate, but it also relies on the high particle impact and velocity in order to create a high quality, dense, and void free coating [7]. Currently, cold spraying additive manufacturing methods have only been used for small components, repair of porous parts, and highly specialized small batch manufacturing. CSAM can be useful in many different applications, which can include manufacturing heat sensitive materials, aerospace component

production, automotive repair, industrial machinery, and marine applications among others [8, 9]. This system offers a variety of different varying applications with the different levels of quality and surface finish. Depending on the feedstock powder used and the manufacturer, there are many pure deposition materials as well as specialized alloys which can be used in CSAM applications [9].

For CSAM additive manufacturing, it is important that the coating powder particles be semi-melted in order for them to undergo proper kinetic deformation upon contact with the surface of the substrate [10]. The density of the individual particles as they stick to the surface of the substrate is important, as the less voids in the coating, the higher quality the coating will be [11]. Voids found in CSAM coatings which can be detrimental to the quality of the coating or component created with this method are called inner-particle boundaries or micro pores [11]. These voids will be analyzed and will determine the overall quality of the final CSAM coating [9].

2.2 Background in Thermal Spraying Processes

Thermal Spraying is a broad categorization of processes which involve the spraying of feedstock metal or ceramic material onto the surface of a substrate. These coatings are generally useful for anti-corrosion, thermal protection, repair or damaged components or surfaces, and improved general mechanical properties. Thermal systems can involve a variety of different feedstock materials and can spray them in many different forms. The most common feedstock forms found in thermal spraying include fine metal powder (atomized), pure alloy metallic feeder rod, and metal in wire form [12]. Some specialized thermal spraying methods also utilize liquid feedstock, which must be prepared in chemical or aqueous solutions to be sprayed onto the

substrate properly [5]. Most thermal spray processes rely on compressed gases or liquid fuel to function properly, compressed air is commonly used in many systems to propagate the material through the system. Other common fuels or gases used in this method include are oxygen, nitrogen and helium, which must be pure and contain no moisture or other impurities [4, 5, 6, 11]. Thermal spraying generally delivers consistent, high-quality coatings and repairs on surfaces, with uniform porosity between the grains, and high density. Thermal coated surfaces have high machinability which is necessary when applied for repair of damaged components. As can be seen in the figure below, under the umbrella of additive manufacturing, thermal spray systems are a broad category of additive manufacturing methods that involve deposition of material onto a substrate with the use of allied energy sources such as high heat and high kinetic energy.

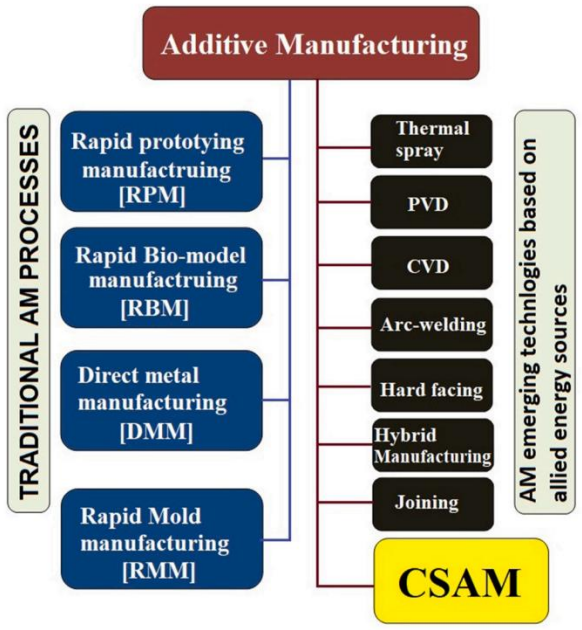

Figure 2. 1: CSAM in Relation to other AM technologies, and other thermal spraying methods [11].

2.2.1 High Velocity Oxi Fuel (HVOF)

High velocity oxygen fuel is a type of thermal spray technique, which as the rest of its counterparts relies on the melting of a deposition material and a compressed gas to deposit the material onto the surface of the substrate [4]. The coatings that are typically generated with the HVOF thermal spray process are typically used in thermal resistance applications and corrosion prevention. Nickel based coatings are common with this oxygen based, high velocity thermal spray as they have a high density and ease of use with this system [4]. As with CSAM cold spray, this process also works in a similar way to where the powder particles undergo plastic deformation as they impact the substrate [4]. Similarly, the high temperature and the kinetic energy of the impact are what makes the HVOF coating similar to CSAM coatings in that they use the same general process. The HVOF process utilized oxygen fuel which can either come in gas or liquid form [4]. Where HVOF differs from other processes, including the cold spray additive manufacturing processes, is that the oxygen fuel is pumped into a secure combustion chamber where it is ignited. The oxygen fuel then mixes with the deposition powder material at high pressure and heats it up to a high temperature as it travels through the system. By the time the material and ignited gas reaches the supersonic nozzle, it is already melted and has reached the desired temperature [4]. Adding a combustion chamber increases the complexity of the system and thus it requires more energy consumption compared to CSAM and other thermal spray methods. The particle size range that is usually used in HVOF typically comes in the sizes of 3-45 μm in size. According to several sources, the particles used are typically carbide reinforcements, metals and alloys [4]. This process makes the particles reach a high velocity similar to that of CSAM of up to 500 m/s, which is considered relatively high in the field of

thermal spraying [4]. In the Figure 2.2, a basic diagram of a HVOF nozzle with different inlets that allow for coolant, oxy-fuel, and the feedstock material and gas combination. These are fed through individual inlets and then mix as the nozzle is converging.

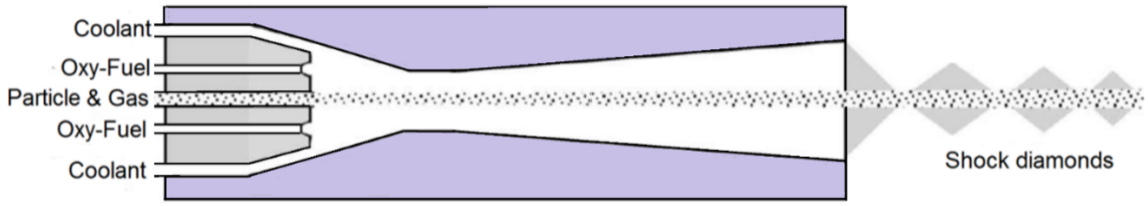

Figure 2. 2. Basic Schematic of a HVOF nozzle with the various pre-chambers in the input area with the shock diamonds created on the output [4].

2.2.2 Flame Spray

The liquid flame process is another thermal spraying process which can create specialized coatings and deposit material to the surface of a substrate. This thermal spray process relies on either chemical or electrical power to ignite fuel which is stored at high pressure in a fuel tank. This process uses a custom-made spray gun with an atomizer, which allows for the solid metal particles to mix with the liquid and the fuel to become liquid droplets. Once the deposition material has become liquid droplets, then they reach a phase where the liquid droplets become solid particles and then they are deposited onto the substrate [5]. The fuel for the flame liquid spray can either be oxygen, or hydrogen gas and it can also be used in a liquid form, depending on the intended application of the flame spray [5]. The deposition material can also come in a variety of ways, which include a rod, a bending wire, or metal that is already in powder form [5]. For flame spray, the depositing material can be used as a liquid feedstock as well as seen in the figure below which shows liquid feedstock and its deposition stages. To achieve a liquified

feedstock material, the metal must be in powder form, and then must be dissolved in a chemical solution, which can be made from aqueous based solutions, or solutions which are based with acetone or alcohol [5]. Once the deposition material is made into a liquid feedstock, it can be used for liquid flame spray [5]. The quality of coatings created with flame spray is relatively high, with a low micro-pore percentage and high density because of the liquid droplets and particles reacting together in the flame as they are being deposited. The particle sizes of the deposited material for this system are micron sized on average, which is relatively good compared to other thermal spray systems, however the desired size for the highest quality is nano-sized particles, which is difficult to do with current flame spray designs [5]. To have the highest quality coatings with flame spray, the system must use an ultrasonic atomizer, which allows for more uniform individual particles. The uniformity of particles when sprayed on the surface of the substrate, will create overall harmonious grain crystal structures, and will have a consistent quality of the surface [5].

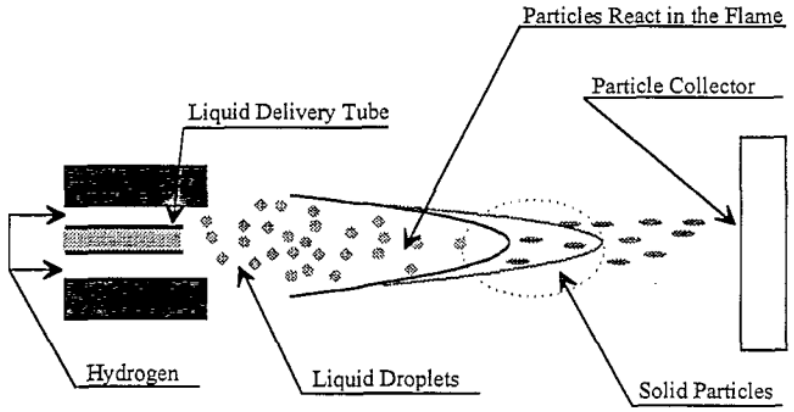

Figure 2. 3 Basic Liquid Flame Spray (LFS) setup with input and output of the nozzle area demonstrated. [5].

2.2.3 Detonation Spray

Detonation thermal spraying is a coating system which allows for the spraying of melted metal powder onto the surface of a substrate. This process leaves high quality results and highly uniform particles are formed in the process. This system however is one of the most complex thermal spray systems, as it relies on many working components to function properly, and involved an internal combustion process, which adds to the complexity of the system. The detonation spray relies on metal powder feedstock that averages on 50 μm in size of each particle [6], and it is moved through the system with high pressure compressed air. The overall system includes compressed air tank, a custom-made spray gun, a control system, powder feeder, water pump, spark plug combustion chamber, and a water pump for cooling purposes [6]. The system works by pumping the powder feedstock into a combustion chamber with a combination of liquid oxygen and acetylene which are fed into the chamber at the same time [6]. A combustion occurs with a spark plug which ignites the fuel mixture and feedstock combination inside the combustion chamber and the material is shot out through the nozzle spray gun [6]. The main propagation of material is due to the high pressure of the compressed air, and the detonation that occurs though the combustion process. This combination of high-pressure air and the detonation with a spark plug is what makes the quality of the coatings made by detonation spray unique and of a high quality [6]. The system however can be costly and difficult to maintain, as these detonations that occur in the combustion chamber are like those that occur inside of engine blocks. The result of the detonation spray are coatings which are excellent for corrosion resistance as well as of a dense quality.

2.2.4 Plasma Thermal Spray

Plasma thermal spray is another thermal spray method which is widely used in commercial and industrial applications as it is great for creating coatings for anti-corrosion and has great thermal protection properties [13]. As plasma spray is a sub-process of thermal spray [13], it has many shared characteristics with other thermal spraying methods. There are several different sub-categories and processes of plasma spraying, which have unique applications and are versatile in many ways. Some of these examples for different plasma spray systems are Air plasma Spray, which involves air at high pressure to move the feedstock powder material into a mix with hot plasma [13], which causes the feedstock metal powder to become melted. The material is then deposited by the hot plasma and compressed air onto the substrate surface. Another different plasma thermal spray system is called Vacuum plasma spray [13], and it works by mixing the feedstock powder in a vacuum with hot plasma and then combining it to have the particles melt and create a fine stream of melted metal, which is then pressurized and applied onto the surface of the substrate as can be seen in the Figure 2.4 [14]. These plasma spray processes rely on fine powder or liquified form of feedstock material and can operate with either ceramic or metallic powders [13]. The overall coating characteristics for plasma spray coatings are dense material deposition areas, with ultra-fine splats of uniform material and average porosity content with high levels of uniformity [13]. The defects which are common with plasma sprayed coatings are un-uniform disposition areas, caused by insufficient pressure or inconsistent plasma streams, and un-melted particles, caused by differences in plasma temperatures [13].

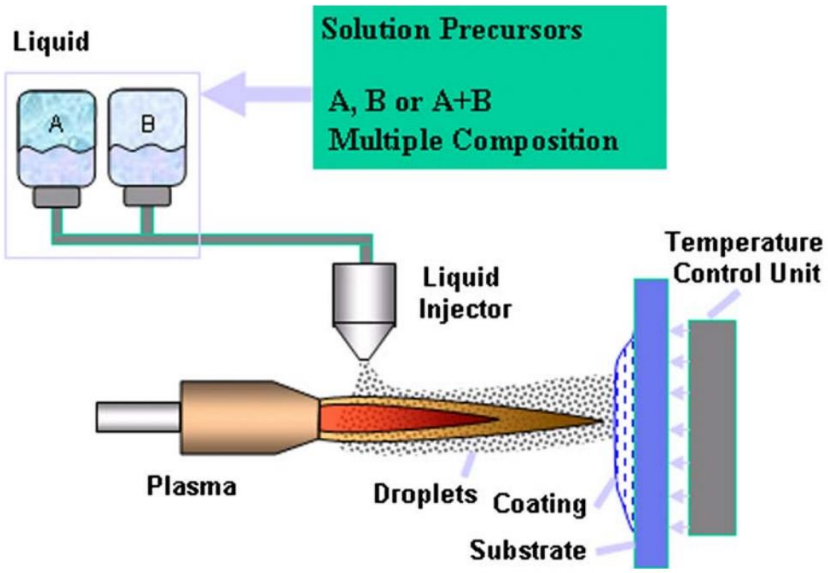

Figure 2. 4. Basic Schematic of Plasma Spray System with input solutions (A, B) and how they are injected through the nozzle at the inlet pre-chamber [14].

2.2.5 Cold Spray

Cold Spray (CSAM) is a sub-category of much wider thermal spraying family, which includes a variety of different processes such as wire arc spray and thermal plasma spray. CSAM uses a method of cold gas spraying which is unique and is one of the most popular methods of thermal spraying which is gaining more attention [11]. This thermal spraying method has the ability to repair and create new components while using less material and energy to operate [11]. CSAM can also be sub-categorized into different types of cold spray, two of which are low- and high-pressure systems, which have distinct uses and results [7]. As shown in the Figure 2.5, CSAM is comprised of relatively few major components and sub-systems. These comprise of a gas/air tank, heating element, central control module powder injector and nozzle. Cold spray systems are usually placed into the low- or high-pressure category by determining if the equipment operating pressure reaches more or less than 1 MPa of pressure. If the system is

operating at >1 MPa of pressure, then it is categorized as a high-pressure cold spray operation [7]. If the operating pressure is <1 MPa, then it is considered a low-pressure cold spray operation. Differences with low and high pressure CSAM systems are also in the configuration of the inner design workings. High-pressure CSAM systems typically start with a compressed gas, and then divert into two separate lines where one line is where the gas meets the feedstock powder and propels it towards the nozzle [7]. The other line of compressed gas goes through a serpentine gas heating element where the gas is heated to a temperature slightly over the output temperature to account for the loss of temperature [7]. The powder and gas mix converges together with the heated gas at the inlet of the nozzle, commonly referred to as the pre chamber [15] where the metal feedstock powder is combined with the hot gas for the rapid melting to begin. The high-pressure then propels this mixture onto the substrate through the nozzle [7]. Low-pressure CSAM systems have a different layout, where the compressed gas/air is heated using a serpentine compressed gas heater, and then the heated gas combines with metal powder in the pre-chamber of the nozzle [7, 15]. These differences in design allow for better use of the different pressure and temperature limitation of the different systems.

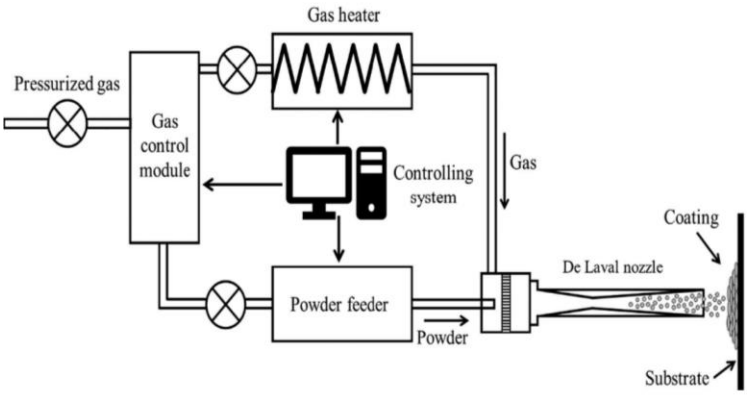

Fig. 2. Schematic diagram of cold spraying process [10]

Figure 2. 5. Basic CSAM System schematic showing the crucial components and sub-systems with a basic layout and a depiction of a substrate being coated with feedstock powder. [16].

As CSAM is a type of thermal spraying, there is heat involved in the process, which causes semi-melting of the atomized spherical powder particles which are the depositing material [11, 10]. This process is referred to as a cold spray because the temperature used is not enough to completely melt the depositing powder material, but merely high enough to get the individual particles to become semi-melted [10]. Cold spray relies on the kinetic energy of the impact that each individual powder particle has on the surface of the substrate. As the individual particles are semi-melted, they become deformed as they impact the substrate. This deformation allows them to create strong inter-particle bonds and creates a dense deposition layer, which is desirable in most cold spray applications [10]. To ensure high density, uniform and high-quality deposition layers, many cold spray machines can be automated, and a uniform deposition rate is set. Slow deposition rates are typically the most desirable, as they allow for denser and thicker layers of material to form on the substrate.

Cold spray technology allows for the customization of the deposition material, which gives CSAM an advantage over other thermal systems which have a limited range of material that they can spray. Powders can be mixed to allow for a coating with unique material properties. Laser-based material deposition techniques have similar results to cold spray techniques, however they often have a hard time with certain materials such as Copper and Aluminum, as their low melting point causes problems with laser equipment. CSAM has the advantage of being able to deposit a wide range of materials with different densities and melting points [11]. CSAM equipment typically have two or more material holders, which allows for the use of different metals to create these alloys. A common problem with using different alloys is that they typically have different melting temperatures, and different particle sizes, which can result in a coating or repair with a high content of micro-pores. Material property inconsistency can result in a bad or

wakened repair and can be known to break during use or final machining [11]. An example of the different qualities of feedstock material available is shown in the Figure 2.6 as different methods of producing spherical powder particles give different results.

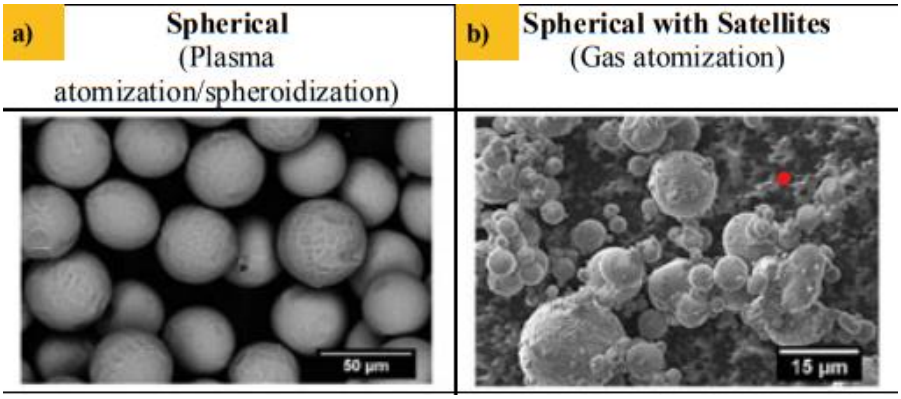

Figure 2. 6. (a) Plasma atomized spherical metal feedstock powder (50µm size) created using a plasma atomization method, and (b) spherical gas atomized metal feedstock powder (15µm size) with satellite particle defects indicating lower quality powder particles [17].

2.3 Cold Spray Additive Manufacturing (CSAM)

As a thermal spray process, cold spray is also considered one of the leading additive manufacturing techniques being used in industry and research. CSAM is commonly referred to as a “solid-state coating deposition process”, as it uses solid state spherical feedstock in powder form. The feedstock powder is then semi-melted and deposited at high velocity onto the substrate surface where it then undergoes plastic deformation [16]. It has many applications, as it can be used to create protective coatings, repair broken components, and even manufacture entire new parts as seen in other additive manufacturing methods. Cold Spray is considered a type of additive manufacturing (CSAM) as it works by adding new material onto existing material, as opposed to traditional subtractive manufacturing, or forming, which removes material from a

solid raw material [18]. Additive manufacturing has many advantages over traditional manufacturing processes used today as it can be more economical and can produce more complex geometrical designs [12, 18]. Using the simplicity of cold spray additive manufacturing and the ease of use of the equipment available has allowed for the diverse range of applications, where there are even examples of CSAM being used in auto body shops to repair crashed cars with standard commercially available cold spray equipment as seen in Figure 2.7 [3]. The flexibility of uses that cold spray has, is due to the range of use of the existing equipment that exists in the market today, as there are a handful of cold spray equipment manufacturers with a variety of different models [3, 8, 9, 19].

Figure 2. 7. An example of CSAM being used to restore a damaged automobile body by adding new material on damaged portion [8].

CSAM has many advantages over traditional flame spray techniques of additive manufacturing, as cold sprayed coatings can better improve tribological and mechanical properties of the substrate [20]. Unlike other thermal spray processes, cold spray relies on low pressure, temperature, and no fuel to create a coating [20]. The lower temperature and pressures that CSAM has compared to other thermal spray methods is that there are fewer residual stresses

on the metal due to rapid heating [18]. The pressure, temperature, and the kinetic energy of individual particles impacting the surface of the substrate create the unique coatings which offer protection from damage from wear, friction, and impacts [20]. The characteristics of CSAM process make this process have overall less energy consumption compared to fuel based thermal spraying processes [20]. Although CSAM can be applied with any metallic powder imaginable, it is commonly used with metals that have a low melting temperature, and softer, [16] which makes it easier to work with using temperatures less than 800 °C [16]. CSAM can create high density coatings by layering the deposition material as seen in Figure 2.8.

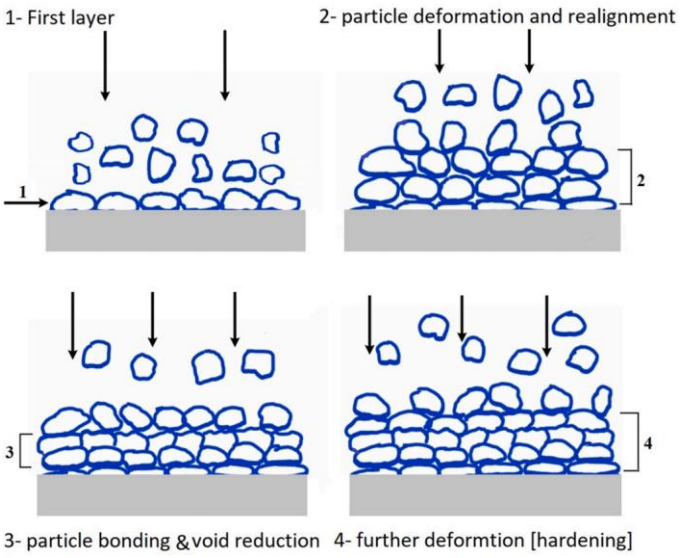

Figure 2. 8. Basic representation of how CSAM feedstock material is deposited onto a substrate and how as the layers of deposited particles create a coating [3].

CSAM has already been applied in a variety of different applications which include aerospace applications for fixing and making aircraft parts [1]. According to the U.S. Military, maintenance related issues have been estimated to cost more than 20 billion dollars per year

alone [1]. Most of the worn-out components are either discarded or relaced, adding to the overall cost. A large contributor to maintenance related problems of equipment is corrosion due to external environments, which can slowly cause metal parts to corrode and become unusable and unsafe [1]. It is known that cold spray has been proven to work flawlessly when repairing aluminum surface components and is known to create coatings that prevent corrosion from damaging the substrate [1]. The low temperatures used in the cold spray process are ideal for softer substrates which may have damage when being repaired by using traditional thermal spraying methods [1]. The U.S. Navy faces many corrosion-related issues with the exposure of navy vessels to seawater, which cause billions of dollars in damage per year as seen in Figure 2.9 [1]. The navy has faced issues with corrosion on valve actuator components, as the exposure to seawater causes porosity on the surface, and quickly renders the component unusable and beyond repair. Cold spray was chosen to repair the surface of the valve actuator to save money on the expensive to replace valve actuator component. After using cold spray to repair the surface of the aluminum valve actuator as seen in in Figure 2.10, they found that the porosity of the cold sprayed area was less than 5%, and after testing several spray angles and particle velocities, they were able to achieve a less than 3% porosity on the surface of the substrate [1]. After the testing of repair using cold spray for the valve actuator, it was determined that repair with cold spray was more economical and offered a higher ROI (return of investment) compared to simply replacing the component with a new one each time it fails due to high corrosion [1].

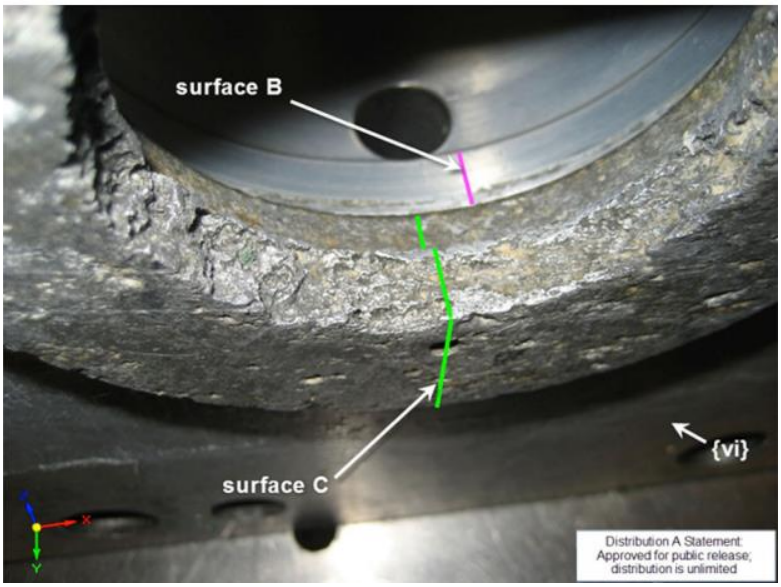

Figure 2. 9. Navy bore actuator before being repaired with CSAM coating, showing extensive corrosive damage caused by exposure to salt-water [1].

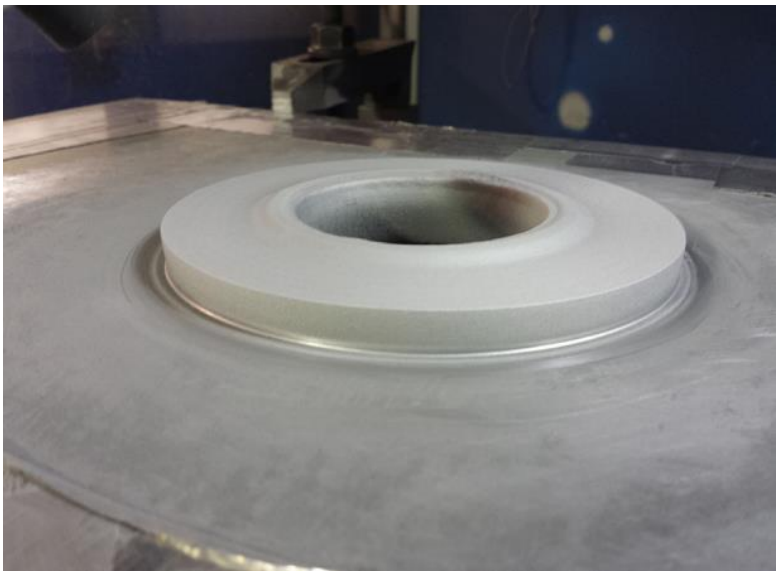

Figure 2. 10. Navy bore actuator after being repaired with a CSAM metal coating which added a new layer of material to the corroded surface [1].

As cold spray has been known to be an economically stable technology for repairs and can even create new components, it is known to have faults in the quality of the coating or

deposition area on a component that if not done with the correct parameters, the deposited material will not be up to standards. Once of the biggest issues faced with using cold spray is that cold spray can have low quality material properties of the coating that is applied over a substrate [11]. These quality issues mainly come from the presence of Inter-Particle Boundaries (IPBs) and micro-pores [11], which can weaken the overall grain structure of the cold sprayed coating on a substrate. These micro-pores can cause cracking and failure of the cold spray deposition area [11]. As it is known, cold spray relies on the individual particles to undergo plastic deformation when impacting the substrate surface as they are semi-melted with the low temperatures. The plastic deformation upon impact is what makes cold sprayed coatings strong and reliable, however if the particles are not sufficiently melted and do not undergo sufficient deformation then the IPBs and micro-pores will be of a higher percentage, causing a low-quality coating [11]. To combat these defects, higher temperatures and pressures are needed to sufficiently melt and accelerate the individual particles so that they undergo the necessary plastic deformation needed to have a high quality cold sprayed deposition [2]. Higher ductility of the feedstock material ensured that the deposition area of the substrate has a high-density coating. These high-density materials which are commonly used in cold spray coatings are metals such as aluminum and copper, which have low melting points, are good heat conductors, and are highly malleable [11].

When working with cold spray, there are three general stages of material deposition which typically occur. The first of which can be noticed as the growth of the initial deposits of material on the surface of the substrate is occurring [2, 11]. The individual particles of material undergo plastic deformation as they impact the surface while in rotational motion. This occurs in individual layers of material deposition. The second stage is that as the particles become layered

on top of each other with the same plastic deformation as they impact the surface [2, 11], the porosity decreases as there is compressive stresses between the individual particles. If the particles have high enough compressive stresses, as they cool, down, they will have high inter-particle bonding resulting in a tight coating with enhanced mechanical properties. The third stage of material deposition is when the individual layers cool and the density if the overall coating increases due to the compressive stress [11].

Several post-cold spray treatments have been devised to improve the overall quality of the deposited material after cold spraying. These post treatments are done mostly to improve the overall porosity/micro-pore content in the coating or repaired area. These post treatments are typically annealing of the cold sprayed material or involve the addition of a heat or pressure treatment to ensure that the quality of the cold sprayed area is high and with minimum pore content (>5%) [10]. The annealing process applied to the cold sprayed area allows for the recrystallization of the material and helps correct any defects with the IPBs [11]. Additional heat treatment can also help with micro cracking which can occur when the impact of the particle impacts a damaged are of a substrate and propagates a crack. Typical CSAM systems do not come with a heat treatment chamber, therefore these additional treatments are usually applied after the initial CSAM process has already been applied and has cooled down and been machined to the exact specifications [2, 8, 9, 19].

2.3.1 CSAM Process/Mechanism

Since CSAM is a relatively new process, that has only been available for a short period of time, the available CSAM systems all share a basic working mechanism which has several stages before the final cold spay [16]. Most CSAM processes rely in a compressed pressurized gas to

propel the feedstock onto the substrate. The pressurized gas usually goes through a gas filter or pressure regulator to ensure the gas is not mixed with impurities that may damage the system. These gases are typically compressed air, nitrogen N_2, or helium (He) gas [1]. Depending on the type of CSAM and the desired operating pressures and temperatures, the gas used differs. Typically, helium gas is used when the parameters call for a higher velocity of the particles as helium has properties which make it work better with higher temperatures compared to air or nitrogen. This is because helium has a higher specific heat and specific gas constant than Nitrogen (N_2) [1]. By using helium gas over nitrogen, the cost can be more as it is more expensive, however if the required velocity, temperature and pressure are relatively high, then it is more favorable to use helium gas over nitrogen and compressed air [1]. For low pressure and temperature cold spray applications, it is more advantageous to use compressed air as it is the most cost effective and easiest to obtain. The gas used also depends on the operating pressure of the system in use, as well as the feedstock metal. For example, one of the systems with the highest operating temperature and pressure range on the market is VRC systems CSAM machine, where it is possible to spray powder material such as stainless steel, which requires high pressure and temperature [1, 19]. Other available systems are incapable of reaching high enough temperatures and pressures to cold spray metals such as stainless steel. Since the VRC system can use both helium and nitrogen gas, it is important to know what the application is and what is the desired output. If the feedstock material requires high enough pressures and temperatures, then helium is better to use. In the example mentioned before, where a navy actuator valve was being cold sprayed, at a pressure of 30 bar, and a 30 mm spraying distance, then with helium, the temperature would have to be set at 25℃ where with nitrogen, the temperature would have to be over 1,000℃ to achieve the same result [1, 19, 21].

As CSAM is a type of thermal spraying, it utilizes a metallic or ceramic feedstock deposition material, which can come in different forms. The most common CSAM feedstock material comes in powder form and is typically found as spherically atomized micron sized powders [22]. These powders can come in pure form or mixed as alloys [16, 23]. One of the main issues with combining different powders in CSAM is that they have distinct melting temperatures and hardness values, if not paired correctly, this can create a weak coating with low quality mechanical properties such as hardness, and low grain density [11]. The metal powders used in CSAM applications are typically sold by the manufacturers of CSAM systems such as the ones shown in the Figure 2.11, sold by VRC Metal Systems, with the most common powders on the market being aluminum, copper, and nickel [11, 16, 19]. Other metal powders that can also be cold sprayed include stainless steel, tungsten, and other manufacturer specific alloy powders [9]. These other metals are rarely used however, due to their high melting temperature, high density, and high cost [1, 16, 21]. Most in-market CSAM machines cannot handle the high pressures and temperatures needed to have these materials reach the required semi-melted state, which is critical when applying the CSAM coatings [19, 23].

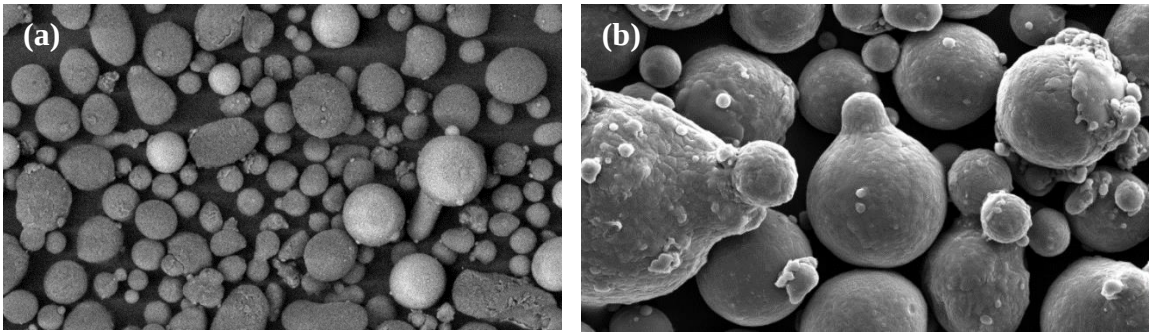

Figure 2. 11. Spherical metal powder feedstock consumables: (a) aluminum 2024, and (b) aluminum 2024-B1 [19].

CSAM requires the metallic powders to be semi-melted, and therefore the systems must have a precise temperature control system where it is possible to regulate the temperature to a high degree of accuracy. Most cold spray systems rely on a heating element in the design to achieve this [16]. The heating of the metal can be achieved in several ways, and depending on the outcome desired, the design of where the heating of the metal powder is crucial to CSAM systems. In many basic systems, a gas heater is used where the pressurized gas passes through the heating element or coil, and then meets the propelled metal powder before it enters the supersonic nozzle outlet [11, 16]. Common heating elements used in cold spray systems are serpentine coil heaters where coils of heating material are organized in a long tube-like chamber [24]. Many of the in-market examples for these heating elements include one or more thermocouples or other temperature sensors which can be attached to a controls system allowing for temperature regulation. Heating can also be achieved by having the metal powder pre-mix with the gas before it reaches the heating element, then the gas and powder pass simultaneously through the heating stage of the system and the powder is already in a semi-melted state by the time it reaches the output supersonic nozzle [25]. The problem with having the gas and powder heated before it reaches the nozzle is that the powder particles may stick together as they are semi-melted and as they travel to the output area, the particles cool down enough to where they begin to harden and cause clogging in the nozzle [25]. Since there is the potential clogging problem, most cold spray designs have the heated gas and powder combine at the supersonic nozzle inlet before being sprayed [25, 26]. A potential issue with having the powder and heated gas mix in the inlet of the nozzle before being sprayed is that it may not be enough time for the powder particles to reach a semi-melted state, therefore causing the output deposited material to

come out as a solid and not coat the substrate correctly. This is the reason why heating elements used in cold spray system designs usually require 3.5 kW or more of electricity to work properly.

The outlet of the CSAM is typically a supersonic De Laval nozzle as seen in the Figure 2.12, which can propel the semi-melted deposition material onto the substrate at high velocities to achieve plastic deformation upon impact on the substrate surface [16]. In the majority of CSAM systems available on the market, the nozzle is directly attached to the end of the heating element to achieve the best results. The nozzle design can be optimized by changing the inlet, converging, and outlet diameters to achieve the desired output velocities. Nozzles can be optimized depending on the type of system they are being used in [25]. Nozzles typically have parameters which can be changed to improve the particle travel velocity at the output. These parameters are the inlet diameter, the nozzle throat diameter, and the outlet diameter, as well as the overall length of the nozzle [25]. When studying De Laval nozzles, it is important to know the exit width, "*h*", and the divergent length, "*L*", these make up the width to divergent length ratio [22]. This ratio is typically found to be about 0.2 in most De Laval nozzle designs used for cold spray applications [26]. It is known that when the width to divergent length ratio is less than 0.2, the energy used is greater because of slower coating rates [26]. The ratio being about 0.2 is ideal for cold spray because it has the least clogging of deposition material and has sufficient enough particle velocity. Other factors that affect the particle velocity are the gas being used, the size of the individual particles, and the type of powder being used [25].

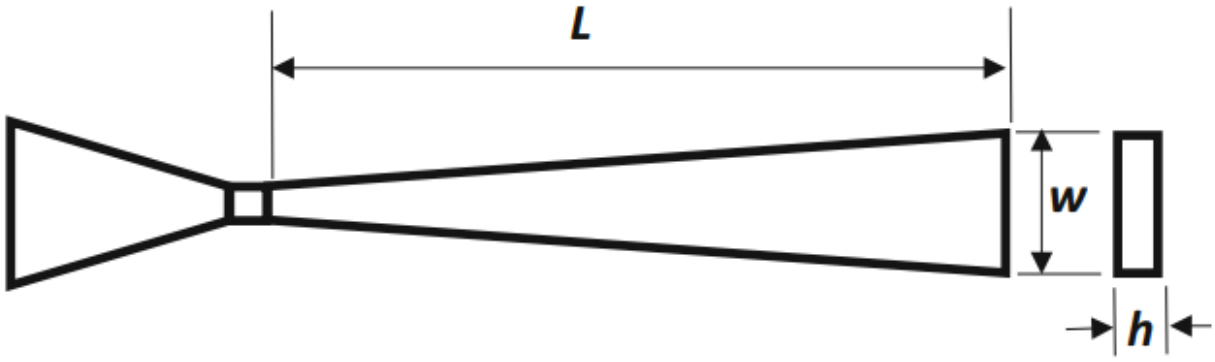

Figure 2.12. A basic geometric representation of the De Laval nozzle which show the relationship between the exit width and the divergent length of the nozzle. [26].

CSAM nozzle design typically has several inlets for the compressed gas, powder feeding, and the sensors required to ensure the temperature and pressure are correct [26]. There is usually a thermocouple placed in the inlet of the nozzle to measure temperature, this ensures that the particles are exposed to enough heat before being propelled onto the substrate surface [25]. It is also important that a pressure gauge is present in the nozzle inlet to measure the pressure levels before output [25]. The area of the nozzle inlet that these inlet areas, and gauges are placed is typically referred to as the prechamber, where all the gas and particles concentrate and build up pressure before being sprayed onto the substrate [25]. The prechamber is normally where the connection to the rest of the system is, this connection is typically connected via a hose to the rest of the system. This can be seen in in the cross section of a CSAM spray gun seen in Figure 2.13, where the prechamber has the gas and powder supply in the inlet of the spray gun.

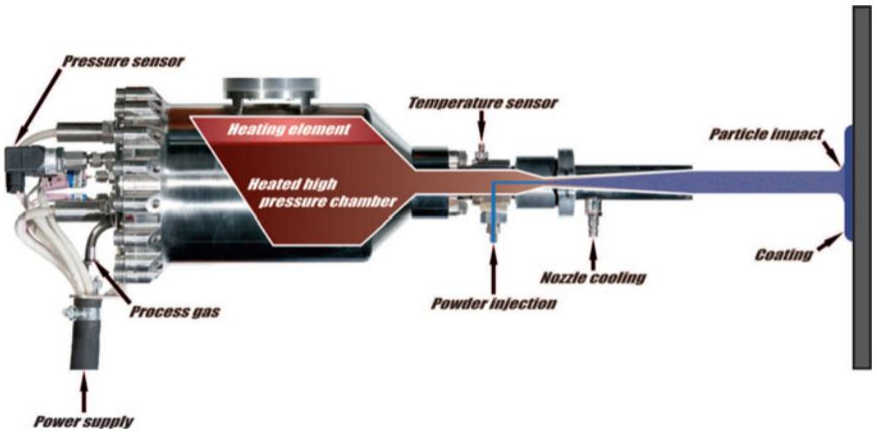

Figure 2.13. A schematic of a complete CSAM spray gun showing the various inlets, hoses, wiring, pressure chambers and nozzle section and how it is typically laid out [17].

CSAM systems use high temperature resistant hoses to ensure that the feedstock material travels through the system at high temperatures without clogging, this can extend the life of the nozzle tube and prevent it from being replaced more often. Some system designs do not require heating at an early stage of the system; however, the hoses still must be able to withstand high pressures. These hoses are usually lined with sensors to measure pressure, temperature, and velocity throughout the different stages of the system [8, 9, 19].

2.3.2 Cold Spray Configuration

In CSAM, there are two main categories of systems, which include HPCS (High Pressure Cold Spray) and LPCS (Low Pressure Cold Spray), which are based on the system pressure at the inlet of the spray gun, which then propels the feedstock material onto the substrate. Both configurations have similar components, however the layout and design can vary depending on manufacturer and the purpose of the CSAM equipment. LPCS systems end to be better for uses in repairing damaged components and creating specialized coatings, as there is less of a need for

sustained operating times and deposition accuracy. For creating new components or components with complex geometrical design such as hollow passages in the surface, HPCS systems are better suited for these tasks as they are typically more accurate in deposition due to the higher temperature and pressures. These HPCS systems are more likely to be used on CNC automatic configurations developed for a pre-programmed spraying operation.

2.3.2.1 High Pressure Cold Spray (HPCS) High pressure cold spray is typically used for high density and melting temperature deposition materials such as stainless steel, and nickel, which have higher melting temperatures and higher density than materials such as aluminum and copper. Systems that are considered high pressure cold spray systems include VRC systems such as Gen III, Dragonfly, and Raptor systems [19]. When categorizing a high-pressure system, the operating pressure of the cold spray system must be greater than 1 MPa to be considered high pressure. These systems usually use a compressed gas of Helium (He) or Nitrogen (N_2) [1] as operating gases. These gases are preferred because they can be compressed to higher pressures and have uniform qualities which ensure constant pressure.

2.3.2.2 Low Pressure Cold Spray (LPCS) Low pressure cold spray systems are used on the shiny metals such as aluminum and copper which are commonly used for cold spray additive manufacturing because of their low melting temperature and malleable properties [26]. Low pressure systems are systems which operate on pressures below 1 MPa, and typically use compressed air, and can also use helium (He) and nitrogen (N_2) however compressed air s usually sufficient for the application used [13]. Typical systems which are low pressure are Dymet 400 series systems and SST Centerline portable cold spray systems [8, 3, 9]. The design for a LPCS can be seen in in Figure 2.14b, where the basic design is simpler than the HPCS seen in in Figure 2.14b.

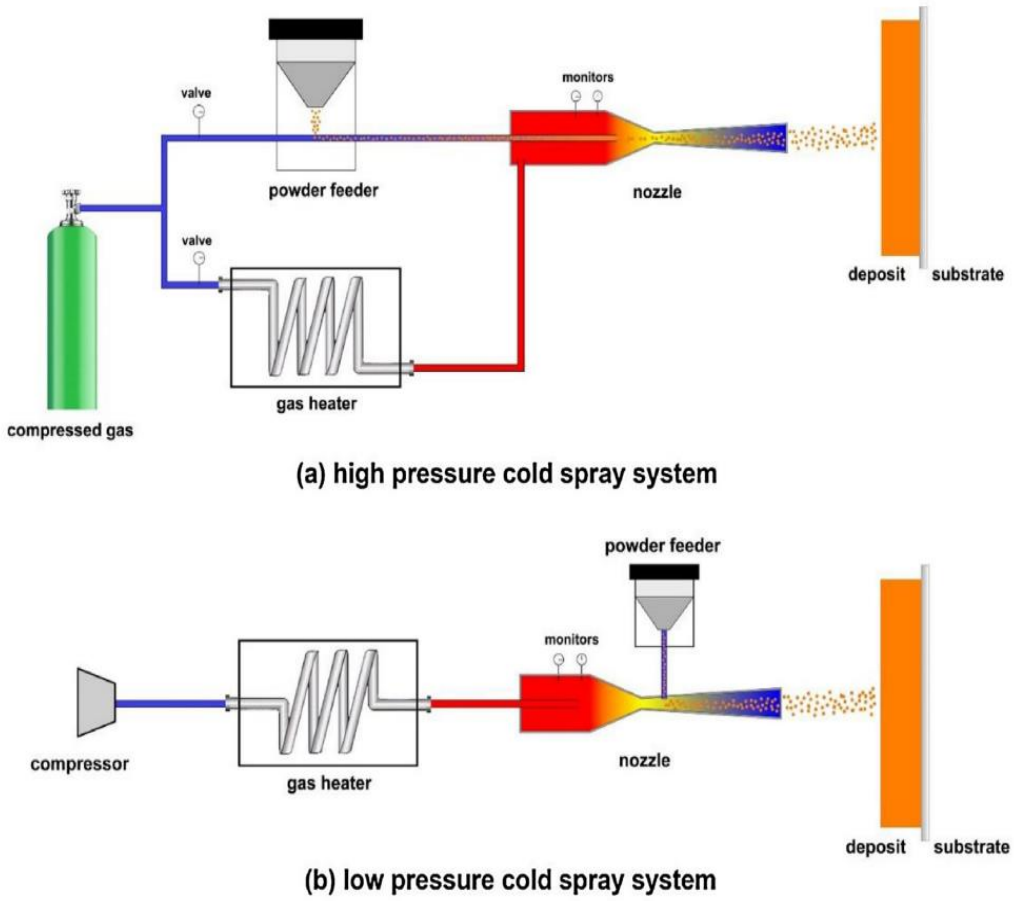

Figure 2.14. (a) High-Pressure CSAM system basic schematic, showing separation of powder feeder and gas heating element. (b). Low-pressure CSAM System schematic showing how gas is heated initially and powder is added at the nozzle [7].

2.4 Commercial Equipment

Since the cold spray additive manufacturing method was developed in Russia by Anatoli Papyrin and his design team, the rights to the original design have been sold to different manufacturers since the 1980's [24]. The process however has only been commercially available since the early 2000's and has very few companies which produce Cold Spray equipment for public use, each with different capabilities and potential uses. Cold Spray is an alternative

method to other thermal spray methods which also utilize metal powder and deposit material in similar in similar ways albeit with higher temperatures or pressures and different deposition methods. The general uses of cold spray additive manufacturing include coating application to prevent corrosion and enhance the mechanical properties of the substrate being coated as well as repair of existing components. Since CSAM deposits materials via a nozzle, and the deposition method is not as precise as a laser or an electron beam, CSAM has limitations on creating completely new components, however, there has been improvements in research for making new parts with complex geometry [18]. CSAM however has shown excellent coating abilities and when used with a CNC automatic system, the coatings can be controlled and deposited consistently [12]. These coatings can have diverse industrial applications which include aerospace and marine components which must be able to resist corrosion and wear. The process is also known to add new material where old material has been broken or damaged, therefore, it is a viable method for the repair of broken critical components in machinery.

2.4.1 Reym Engineering CSAM Portable System

Figure 2.15. Reym Air Engineering Technology CSAM System [27].

The Reym Engineering cold spray systems are manufactured in Kiev, Ukraine [27] and come in many different model forms which all have different cold spray capabilities. These

systems work with compressed air and can also work with nitrogen or hydrogen depending on the required needs of the customer [27]. The system includes powders feeder containers, a spray gun, powder feeder tubes, and a control system for the air pressure and output powder temperature as seen in Figure 2.15. Just as in the Dymet systems, the Reym system spray gun also includes a connection port for the powder and pressurized air as well as a power cord for the heating element inside the spray gun. Some of the models for the Reym cold spray system do not include the pressure regulator/dehumidifier on them, therefore it is up to the customer to install one. The specifications for a dehumidifier for this specific system are that it has a compressed air capacity of 0.45 m^3 / min [27]. The heating element is a serpentine style coil heating element for compressed air. The spray gun also comes with easily replaceable nozzles which can be replaced if clogging of material occurs or if they don't function at the best capacity due to the rapid heating and cooling. The Reym system is considered a low-pressure cold spray system as it operates with a maximum temperature of 600°C [27]. As in cold spray systems a low-pressure system is a system that operates with less than 1 MPa of pressure, this system is classified as a low-pressure system because it operates at 0.9 MPa of pressure [27]. The power requirement for operation of this system is 220 Volts [27], meaning that it must operate using a special outlet for industrial machinery, this affects where the machine can be used.

Reym also sells the necessary metal powder for its own operating systems, which it recommends be used instead of other manufacturer's metal powder that may not be up to the standards required for the Reym cold spray system. The powders available can either come in alloy form or in pure form, with alloys being some of the most popular powders on the market [27]. The powder supply rate for this system ranges from 2 grams/second to 8 grams/second, which is typical for a low-pressure cold spray system [27].

The Reym Gas Dynamic Cold Spray system is one of the smallest commercially available systems on the market, making it highly desired among cold spray customers. The system has many general uses ranging from automotive repair to aerospace and specialized coatings on components. Reym also manufactures and sells the replaceable nozzles which are used in the tip of the spray gun, these nozzles are also used on the Dymet 400 series systems.

2.4.2 Dymet 400 Series

Figure 2.16. Dymet-423 CSAM System with dual powder canisters [3].

A common commercially available CSAM system is called the "*DYMET 400 Series Systems*", which is manufactured by the Dymet company which is headquartered in Russia with collaborations in Estonia, Turkey and Ukraine. This operating system is a basic cold spray system which can spray two different metallic powders onto any substrate. The system includes a spray gun as seen in Figure 2.16, which must be manually used by a human user. This type of system is considered a low-pressure cold spray system as it requires comparably lower pressures of about 1.2 MPa (12 bar) [28]. These series of machines, all include a pressure regulator controlled via a knob which also serves as an air dehumidifier. The Dymet systems as is typical

of low-pressure cold spray systems operates with normal compressed air stored in a separate air tank. The Typical operating temperatures used in this equipment are also lower than others and can range from 200-600°C caused by a powerful 3.5 kW heating element found in the spray gun mechanism [3, 8]. The system has several variants which all work in a similar way to each other, these variants include, No. 404, 405, 412, 421, and 425 cold spray systems. The price of the Dymet systems can very anywhere from about 300,000 to 600,000 Rubles depending on the model and operating pressures and temperatures [3].

The Dymet System operates by moving the metal powders through a series of tubes which are moved by pressurized air at a constant pressure, as the powders are moved through the system, they are heated with the heating element to a semi-melted state. Once the powder particles reach the desired semi-melted state, they are pushed through a converging diverging supersonic nozzle which is attached to the spray gun, which in turn controls the output of the cold spray onto the substrate. The spray gun is comprised of a compressed air heating element, which is a serpentine style heater with a thermocouple temperature sensor at the output. The spray gun also has a converging diverging nozzle with a replaceable nozzle tube at the end for further accuracy and concentration of the output deposition material [3, 8].

According to the Dymet company, the variety of applications which the system can work on are numerous, and include correcting casting defects, repair of worn-out bearings and restoration of metal components [3, 8]. This system also has the ability to create metal powder surface coatings which can improve resistance to corrosion, flame retardant coatings, and even anti-seizure coatings which can work alongside any lubricants in a mechanical system [8].

2.4.3 SST Centerline Cold Spray System

Figure 2.17. Latest Generation SST system with dual canisters [9].

The SST Centerline company manufactures cold spray coating systems which have high range of uses un the automotive, aerospace and defense industries which require high quality coatings which can undergo tough conditions [9]. These coatings can enhance the mechanical properties of the substrate by ensuring high bond strength between the powder particles in the coating, high density of the grain, and low oxide entrapment which means low void percentages- [9]. The SST company has two main models for cold spray (CSAM) machines, which are the PX and EPX systems, each with different capabilities and ranges of temperature and pressure. Both systems are proven to prevent material deposition clogging in the nozzle area, as well as 120 gram per minute powder feed rates which are an improvement over the previous generation's feed rates of 80 grams per minute [9]. Similar to the Dymet 423 CSAM system, the SST systems

both feature two different powder canisters as seen in Figure 2.17, which boast the ability to swap spray powder material in under 10 minutes [9].

The PX SST system operates at a lower range of powder feed rates and pressures compared to the EPX system also made by SST, however it offers both an automated and manually operated spray gun [9]. This system offers a said temperature range of ambient temperature, to 550°C which is the same temperature range as the EPX system. The pressure ranges of the PX system are 7-17.2 bar (100-250 psi), [9] which makes it have a higher-pressure range compared to the Dymet System. The powder feed range for the PX system is 6-36 g/min, which is a lower range compared to the EPX system.

The EPX system, which is slightly larger and heavier than its PX counterparts has the same temperature range of ambient-550°C. The pressure and powder feed rates on the EPX system are 7-35 bar (100-500 psi) and 12-80 g/min [9]. These ranges are better than the PX system which allows this system to be used in more diverse applications but consume more power as this requires 480 VAC of power compared to the 240 VAC of power consumed by the PX system [28]. The EPX is also limited in that it only has a manual spray gun.

The supersonic nozzle for both systems is made from high quality stainless steel, and it is a converging diverging nozzle [9]. The manual and automatic spray guns have differences in parameters, as the automatic spray gun relies on a 4.25 kW heating element compared to the manual spray gun's 3.8 kW spray gun which is less powerful, accounting for a difference in temperature ranges if using the automatic and manual spray guns. The spray guns are manufactured with weight saving and durability in mind, and they feature high quality impact resistant polymer shell and stainless-steel bodies to ensure durability [9]. The spray gun design is a complex design which was optimized by using numerical models using a variety of different

approaches and equations to optimize and understand the physics behind the design. The nozzle design consists of a miniaturized nozzle design which was specially built to meet design specifications [15]. As in previous systems, the heating element is a serpentine compressed gas heater which is high powered and able to heat compressed gas quickly. It is equipped with a standard thermocouple [15] heat sensor near the nozzle inlet which relays the temperature to the control system in real time. It also comes with a specially designed nozzle along with a powder injection tube at the opening of the nozzle [15]. This allows for the heated gas and the powder particles to combine at the inlet pre-chamber of the nozzle [15].

2.4.4 VRC Gen III Portable CSAM System

Figure 2.18. This is the Gen III Portable Cold Spray System [19].

The Generation III Portable High-Pressure Cold Spray System manufactured by VRC metal systems is a high-quality cold spray system which is capable of running in high pressures and has the capability to work with any cold sprayable metal powder available. This system has a highly maneuverable spray gun which must be used manually as in the SST EPX, and Dymet 400 series systems [3, 8, 19]. This system is highly configurable as it can have the heating element removed easily and can have different reaching distances. The system also has the

ability to operate with air, nitrogen, and helium gas, which gives it more varied working conditions. The temperature ranges in which this system can operate are largen than the previously mentioned systems. The Gen III system can operate in a range of temperature of ambient temperature to 650℃ [19]. The energy consumption of this system is the same as the SST EPX system which consumes 480 VAC of electricity. The metal powder feed rate range is also high, with 1.3-9.3 cm^3 /min which gives it diverse capabilities and makes it useful for many applications [19]. This portable system can also be attached to a spraying booth for added safety.

2.4.5 VRC Metal Systems Dragonfly Cold Spray System

Figure 2.19. VRC Metal Systems Dragonfly Cold Spray System [19].

The VRC metal systems dragonfly cold spray system is a in-market available system meant to be portable and easy to use. The heaviest component of the system has a weight of 39.91 kg and is meant for small specialized critical components [19]. This system is similar in parameters to the other available VRC metal systems for cold spray; however, it is much smaller and specialized. This system can be easily configured by removing components and taking data. This system relies on handheld and remote operators which allow for automated use from a

distance [19]. This diverse system can create cold spray coatings, just as well as it can be programmed to create structural components by depositing cold sprayed material in layers [19].

2.4.6 VRC Metal Systems Raptor CSAM System

Figure 2.20. VRC Metal Systems Raptor System Funded by U.S. Department of Defense (Available after 2019) [19].

The VRC Metal Systems Raptor cold spray machine shared components and capabilities with other VRC Systems and has been used for defense purposes in the United Stated and Australia [19]. This system is larger than previous systems but can deliver consistent coatings with high density of the deposited material due to the high pressures. The Raptor and Dragonfly systems both have recent technological advancements which allow for Helium recovery for it to be reused at the same consistent pressure. Currently, these systems can recover about 90% of used helium gas [19]. By using helium gas as the main pressurized gas, this system has enhanced abilities for the development of advanced structural repair with high density volume of the deposited material. Apart from Helium, both the Raptor and Dragonfly cold spray systems can be

made to use onsite Nitrogen (N_2) or compressed air [19]. This allows for VRC Metal Systems cold spray machines to be versatile compared to other existing systems on the market.

2.5 Metal Matrix Composites

Metal matrix composites (MMCs) are a special sub-category of composite materials, in which as opposed to traditional composite materials where there is a polymer based soft matrix paired with a metallic fiber, the matrix in this case is a softer metal paired with hard ceramics to add additional reinforcement. In cold sprayed coatings with metal matric composites as the deposition material, aluminum is typically used as the metal matrix as it is ductile and does not corrode very easily [29]. MMCs can result in enhanced mechanical, tribological and anti-corrosive properties due to the addition of high strength ceramics [30]. In CSAM, the bonding of deposition material onto the substrate surface is due to the high-velocity impact of the individual semi-melted powder particles onto the substrate surface. As the particles begin to create layers of deposition material, there is mechanical interlocking between them causing a strong bond [30]. The addition of high strength ceramics to a metal powder CSAM matrix must have a balance of matrix to non-metallic material, as too much can result in erosive effects on the substrate surface and having too little non-metallic reinforcement can result in reciprocal synergy between the materials as is required for a coating with a low pore content [30]. As shown in Figure 2.21, there are several different possible outcomes for the addition of non-metallic ceramic reinforcement added to the metal matrix of a CSAM coating [30]. These stages of spraying metal matrix can be seen in the Figure 2.21 below, where the particle impact is shown. As it can be seen, the ceramic reinforcement which in the case of this research is alumina, with a nickel matrix, it helps compact the metal matrix particles upon impact, and it can help get rid of IPBs (Inter Particle Boundaries) which are micropores in the coating surface.

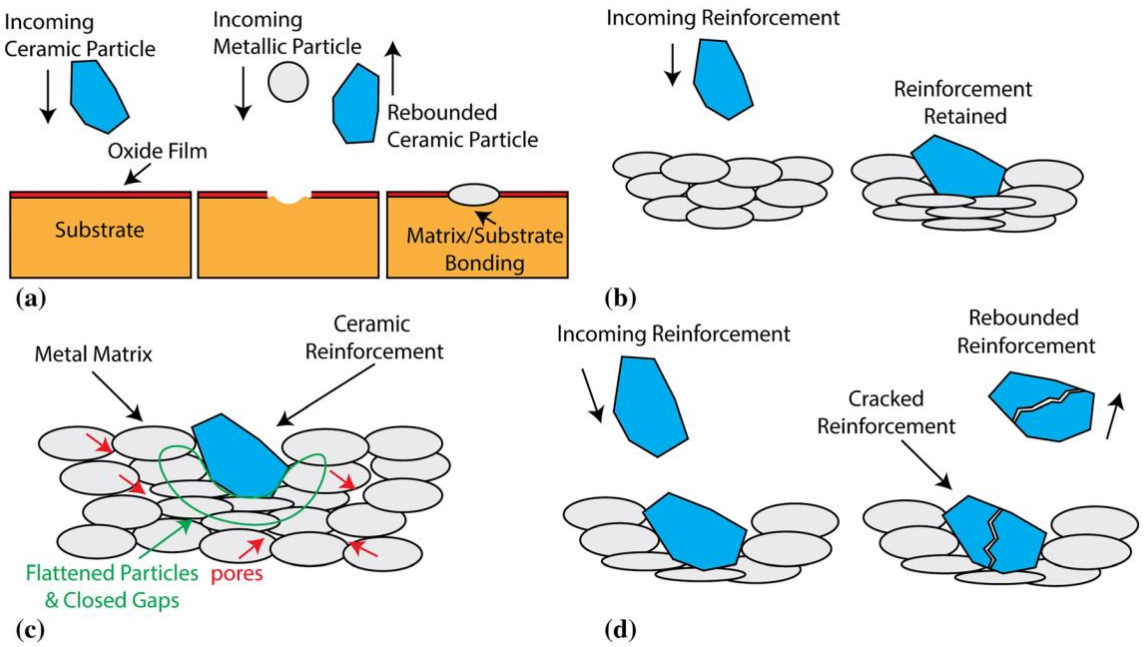

Figure 2. 21: (a) Initial deposition of metal matric particles with ceramic reinforcement particles. (b) ceramic particle compacts layered metal matrix particles. (c) ceramic reinforcement and strengthening of the coating. (d) cracking of ceramic reinforcement [30].

In a study which analyzed how a cold spray coating with the metal matrix of 316 austenitic stainless steel reinforced with alumina (Al_2O_3) ceramic particles, it was concluded that after analyzing the cross section of the coating, there was a higher density coating compared to coatings without ceramic reinforcement [31]. This was theorized to be due to the peening effect on the deposited metal matrix material which is caused by incoming reinforcement compacting the deposited material further [32]. This effect can be seen in the Figure 2.21b above, where the ceramic reinforcement particles create a shot peening effect on the coating surface. When testing the wear rate of the metal matrix composite with 316 steel and alumina Al_2O_3, the results after observing the surface pointed to adhesive type wear [32], which means that there is material transfer between the two rubbing surfaces. This could be because the matrix material is 315 steel, which has a high hardness, being reinforced by the alumina Al_2O_3 particles. Because 316 austenitic stainless steel is already a hard metal, it makes it difficult to measure the improvement

of the wear resistance with the addition of alumina Al_2O_3 compared to metal matrix materials that are softer such as aluminum 6061.

In another study involving MMCs, the powder tested was a Nickel (Ni) Alumina (Al_2O_3) powder, which was created using a hydrothermal hydrogen reduction method [33], the effects of vacuum heat treatment were tested. The samples were tested at 25℃ and 400℃ to further understand the effect of oxidation and annealing of cold sprayed MMCs on the tribological and mechanical properties of the cold sprayed coatings [33]. After performing tribological wear testing using both temperatures during ball-on-disk testing, the higher temperature oxidized coating performed better than the lower temperature coating left that was not annealed [33]. When testing the wear of the MMCs, it was noted that as the matrix metal material wears away, it can leave the ceramic reinforcement material exposed which can create a rougher surface and thus a higher coefficient of friction [33]. For the surface of the oxidized coating, the shearing between the steel ball and the MMC coating didn't not leave as much wear debris and was smoother than the sample that was tested at 25℃. There was a noticeable wear shown on the steel ball used as a counterpart wear surface in the ball-on-disk tribological testing [33].

CHAPTER III

METHODOLOGY

3.1 Introduction

This chapter includes a comprehensive description of the methodology followed to fulfill the objectives of the present research project. The methodology consists of the sample preparation processes, the CSAM coating process, and all the analytical methods used to characterize the CSAM coatings, including SEM (Scanning Electron Microscopy) and microhardness to analyze the coatings surface properties and microhardness testing to evaluate the coatings' mechanical properties. In addition, the micro-abrasion and pin-on-disk techniques used to determine the tribological characteristics of the coatings will be described in depth.

3.2 Substrate Sample Preparation

In the development and analysis of the different CSAM coatings, the substrates used will consist of 0.5 in thick aluminum 6061 (Al6061) disks and 0.5 inches long aluminum rectangular blocks which can be seen in the Figure 3.1. These substrates were chosen to be used in pin on disk tribological testing as well as microhardness, and SEM analysis of the mechanical properties. The substrate samples will be made by cutting them to the 0.5-inch desired thickness with a band saw, and then finishing them with a lathe to ensure consistent surface quality.

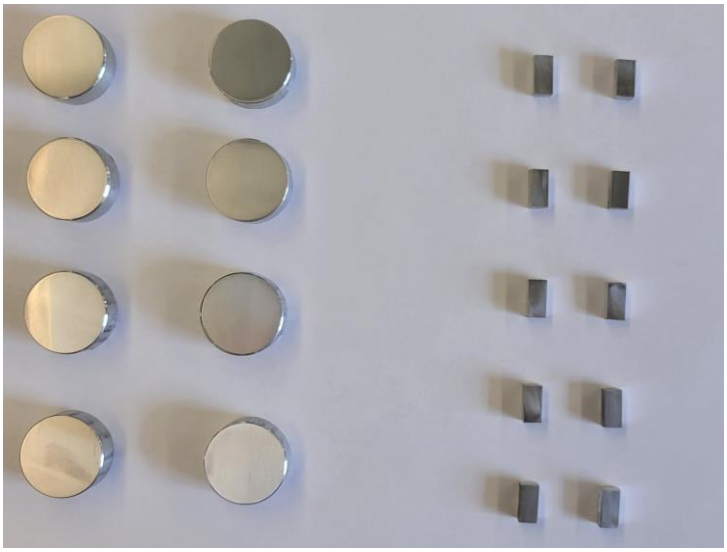

Figure 3. 1. Aluminum 6061 (Al6061) discs and blocks samples after being cut and polished in preparation for the CSAM coating process.

3.2.1 Sample Cutting Procedure

To make the samples, the process begins with raw material 6061 aluminum rods for the disk and block samples. The first step to making them is to measure the samples with a dial caliper and mark the area that will be cut with the band saw at a little over the 0.5-inch mark to allow for the machining in later steps. It is important to not cut the samples to a smaller size below 0.5-inches as this may cause the sample to be smaller after it is machined leading to problems with consistency. To achieve consistent 0.5-inch-thick samples, a useful tip for consistent sized samples is to use a “stopper” as seen in Figure 3.2b, on the band saw so as to cut the aluminum rod at the same distance in every cut, and not having to measure for each cut and risk having an error. As aluminum is a relatively soft metal, to avoid a defective cut, it is recommended to set the band saw to cut at a slow and steady rate while closely monitoring it as it is cutting to avoid quality issues.

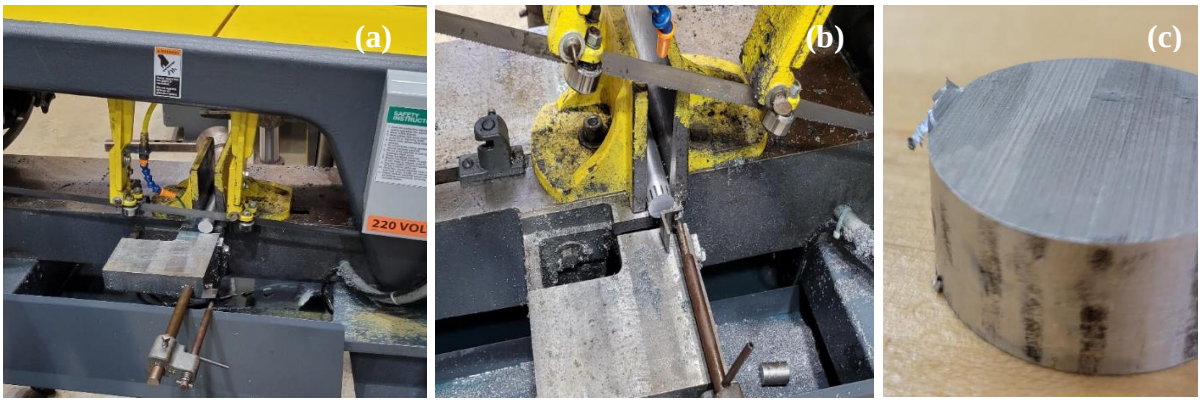

Figure 3. 2. (a) Cutting stage of sample preparation with the band saw, (b) A sopper being used to align the sample and get a consistent cut every time, and (c) disk sample after being cut with the band saw, with a noticeable rough surface saw marks and rough edges.

After the cut has been made, it is almost inevitable that there will be a rough surface with saw marks left behind, and therefore it is important to fix it and leave a smooth surface. To do this, the disk samples are to be "faced" to smooth out the rough saw marks left behind as seen in Figure 3.3a. Another common defect left by the band saw on the disk samples is sharp edges as material was deformed during the cutting process. To fix this, the side in which the sample will be coated with the CSAM coating is "chamfered" on the sharp edge with a 45° chamfer, eliminating the rough edge as seen in Figure 3.3b.

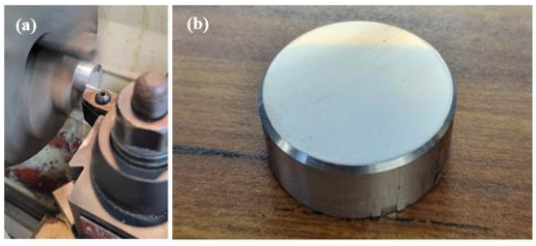

Figure 3. 3. (a) Rough Aluminum 6061-disk sample being faced on a lathe to improve the surface quality before polishing, and (b) Al6061 disk sample after having the rough edges chamfered to a 45 degrees angle.

The block samples have a relatively small surface area compared to the disk samples; therefore, they do not need to undergo a machining process as the disk samples, and to have a flat and consistent surface face, the faces are flattened using the milling machine. The samples are to be faced with the vertical polisher machine running across perpendicular to the axis of the rectangular block samples.

3.2.2 Sample Polishing Process

For both the block and disk samples, the polishing process is similar, as both are made of 6061 Aluminum alloy raw material, which were cut and subsequently machined to create a smoother surface and ensure the samples are all the same size. With aluminum, the polishing standards were followed to achieve a smooth surface on the samples to ensure a consistent surface finish with all the samples. According to standards noted by "Pace Technologies" for 6061 Aluminum alloy, the samples must undergo four main stages of different grit polishing padding to achieve a smooth surface finish of the samples [35]. The first three main stages of polishing consist of polishing on a spinning polisher with water as the only lubricant [35]. The force acting upon the samples can vary between 5-10 lb. of force [35] as the aluminum is relatively soft and easy to polish compared to harder metals. Since aluminum is soft, it is important to note that any uneven application of force on the samples as they are being polished can cause an uneven surface to develop as one side has been worn away more than the other. According to the standards for polishing, the samples must be polished with the spinning polisher set to 100 rpm with water running on the polishing pad to act as the lubricant. The first stage of polishing requires two sub-stages of polishing pads, which are of P120 and P220 grit polishing paper pads each. Another important step to consider is the application of the polishing pad onto the polisher machine, as

sticking it to the surface all at once can cause air bubbles to be trapped under the polishing pad, causing an uneven surface, and making it more difficult to polish the samples correctly.

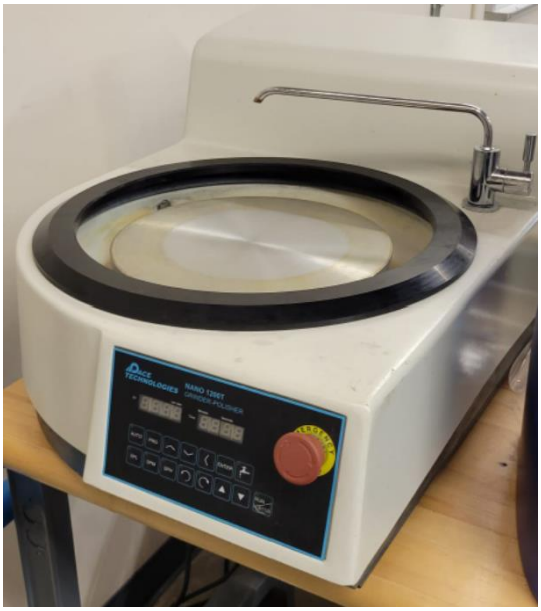

Figure 3. 4. Pace Technologies NANO 1200 T polishing station used to polish disk and block samples.

Figure 3. 5. Difference in surface quality between a machined Aluminum 6061-disk sample (*left*) and a polished disk sample (*right*).

3.2.2.1 Block Sample Polishing Process When polishing the block samples, it was important to figure out the best way to securely handle each sample without causing the blocks to slip and fall into the polisher. As the blocks are small, it proved to be difficult for them to be handled by hand without them slipping away or becoming polished unevenly. The solution for this was to hold them using a pair of pliers and holding them directly over the spinning polishing pad at the indicated spinning speed using only water as the main lubricant [35].

3.2.2.2 Disk Sample Polishing Process For the disk sample polishing process, the process remains like the polishing of the block samples. Since the disk samples are much larger and easier to handle than the smaller block samples, they were held down by hand onto the polishing machine with between 5-10 lb. of force acting onto the center of the disks to ensure an evenly polished surface. Each surface was polished for about 1 minute with each different grit paper polishing pad specified by the standards for polishing aluminum [35]. To achieve an even polishing of the surface of the discs, the technique employed was to use the “Individual force mode”, [35] technique to polish the discs. This means that the discs were placed on the edge of the circular polishing pad and held down in the same position throughout the polishing process. This is different from the “central force mode” which would place the center of the disk sample to the exact center of the spinning polishing pad. It was important to use the individual spinning force method, as this would leave streak polishing marks facing in the same direction. Once the polishing with one of the polishing pads was over, the next polishing pad was placed on the polisher. When using the next polishing pad, the sample was placed to where the polishing grains would run perpendicular to the previous polishing streaks. This technique allowed for the user to know when to stop polishing as the previous perpendicular streaks were not visible anymore.

3.2.3 Deep Cleaning of Samples

After the samples were cut and polished with the P1200 grit ALO polishing paper, the samples were cleaned in a standard deep clean process designed to rid samples of any contamination. The cleaning process is done using an (30I Ultrasonic Cleaner) VEVOR (Vevor, Cucamonga CA, USA) which is filled with warm water and vibrates for a set amount of time. The samples are first placed into sealed glass containers completely submerged in acetone. This will deep clean the pores of the samples and free it of any contaminants. The container is then placed into the water bath in the ultrasonic cleaner for five minutes for a deep clean. For safety reasons, the samples then must be taken out with special tongs to avoid the acetone. They are then placed in a separate container filled with isopropyl alcohol to be rid of any excess acetone. Once this is done, the samples are then placed into the ultrasonic cleaner again for five minutes. Once they have been cleaned, they must be left to rest for at least 24 hours in an environment with minimal contaminants such as dust or excess humidity.

3.3 CSAM Coating Process

The CSAM Nickel coatings will be sprayed on the Al6061 samples using spherical gas atomized Ni powder (CP-Ni) and nickel-alumina powder (Ni-Al_2O_3 mixture) with the mean particle size of 0.5-45 μm. The powders will be sprayed using the PX Series SST Cold Spray System (Centerline (Windsor) Ltd., Canada) with Robotic Gun application, and nitrogen as a propellant gas at a temperature of 500°C and pressure of 205 psi. The standoff spray distance was 12 mm during the coating process with a 20 mm/s gun traverse speed and 1.2 mm stepover per pass. The main characteristics of the nickel powders are shown in Table 3.1.

Table 3. 1. CSAM Nickel powders characteristics.

Material	Catalog No.	Composition Purity	Particle Size (μm)
Ni powder (CP-Ni)	SST-N5001	Ni. 99.7% Min.	0.5-45 ±5
Ni-Al_2O_3 mixture	SST-N0036	Ni. 99.7% Min., Al_2O_3 92% Min.	0.5-45 ±5

3.4 CSAM Coatings Characterization

3.4.1 SEM (Scanning Electron Microscopy) and EDS

The CSAM Nickel (Ni) and Nickel Alumina (Ni-Al_2O_3) coated aluminum block samples' cross section were analyzed using a Field Emission Scanning Electron Microscope (FE-SEM) ZEISS SIGMA VP (Carl Zeiss SBE, Thornwood, NY, USA) seen in in Figure 3.6. This provided information about the coating thickness by measuring the distance between the substrate's surface and the coating surface of the cross section. The SEM analysis also yields an accurate image of the coating grain structure and helps identify any IPBs (Inter-Particle Boundaries) and substrate coating adhesion on contact. Figure 3.6 shows the SEM equipment used to analyze the CSAM coatings.

Figure 3. 6. Field Emission Scanning Electron Microscope (FE-SEM) ZEISS SIGMA VP system used to characterize the Al6061 block samples coated with Nickel (Ni) and Nickel Alumina (Ni-Al_20_3).

3.4.2 Microhardness

To analyze the mechanical properties of the coatings, microhardness tests were done on the surface of the samples using a Vickers Microhardness tester (HMV-G Series Micro Vickers Microhardness Tester, Shimadzu, Japan) shown in the figure below which created a pyramidal indentation on the coated surface of the aluminum 6061-disk samples. The hardness was then determined by measuring the two diagonals of the indentation and calculating the Vickers hardness from those dimensions. The hardness values were then calculated automatically by the system and displayed on the monitor. The figure below shows the microhardness equipment used to take microhardness data.

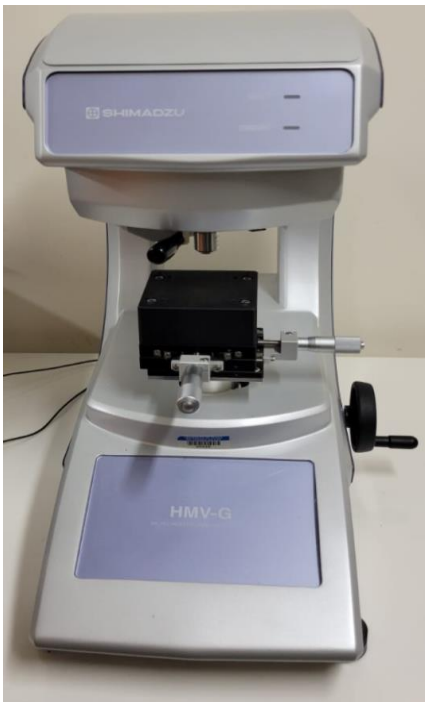

Figure 3. 7. HMV-G Series Micro Vickers Microhardness Tester used to gather the microhardness data.

3.5 Tribological Characterization

3.5.1 Micro-abrasion Tests

The micro-abrasion tests were performed utilizing an Anton Paar Compact CAT2c Calotester (Anton Paar GmbH, Graz, Austria), shown in Figure 3.8. The experiments were carried out following the European Standard EN 1071-6:2007 [28]. This method has been used to evaluate the wear resistance of different coatings [34, 38]. The tribosystem consisted of a rotating steel ball propelled by a rotating shaft onto the surface of the sample, in the presence of slurry with abrasive particles. Coating and substrate wear rates (k_C and k_S) were determined form the tests using the non-perforating of the coating method.

Figure 3.8. Anton Paar Compact CAT2c Calotester.

During the micro-abrasion test, a steel ball is rotated against the specimen in presence of a suspension of diamond abrasive particles. The rotating steel ball leaves a crater. The wear scar or crater produced on the specimen surface is assumed to reproduce the spherical geometry of the ball [36]. By making a series of these craters and measuring the outer diameter as seen in Figure 3.9, the coating wear coefficient, k_C, can be determined from the tests using the non-perforating method [36, 37]. Figure 3.9 shows a representation of how the wear crater is measured to obtain the b_{perp} and b_{par} distances and to determine their average, b, which is the total diameter of the wear scar [28, 38].

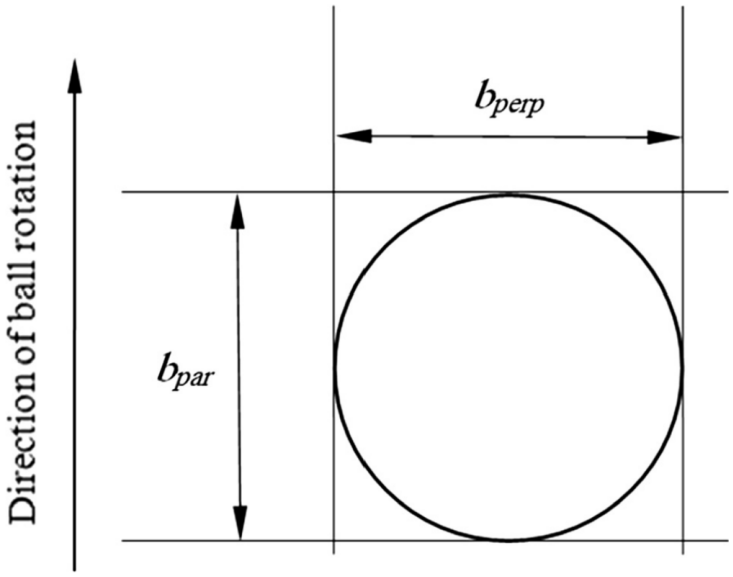

Figure 3.9. Measurement of crater using the no perforation of the coating method [28, 39].

During this test, perforation of the coating does not occur, and using the data collected, the specific wear rate of the coating, k_C, is determined using Eq. 1 seen below.

Eq. 1:

$$k_c = \pi * \frac{b^4}{64RSN}$$

In the equation for specific wear rate, the b is the wear scar diameter, which is calculated by the average of b_{per} and b_{par} as shown in Figure 3.9 [28, 39], R is the radius of the calotte test sphere, S is the sliding distance, and N is the normal force acting on the surface of the sample due to the sphere resting on it.

Before beginning with the micro-abrasion tests, the specimens were ultrasonically cleaned for 15 min, and then rinsed in clean acetone and ethanol. A set of three wear craters were produced in each sample, corresponding to four different numbers of ball revolutions: 400, 600,

900, 1200, 1500 and 2000. The micro-abrasion testing was done using a 30 mm hardened steel sphere (SAE 52100) at an angle of 30 degrees, as shown in Figure 3.10, and the abrasive slurry used was a water base diamond suspension with diamond particle sizes in between 0.5 and 1 microns.

Figure 3.10. A Calotte setup at 30° angle with a nickel coated disk test sample and a 30 mm steel sphere, resting on the rotating shaft and leaning against the surface of the nickel coated sample.

For the experiments, the ball rotational speed was set at 0.2 m/s (130 rpm for a 30mm diameter ball). The normal force, N, acting on the surface of the sample from the weight of the ball was calculated to be 0.54 N. To determine the wear coefficients for each sample, the

diameters of the wear craters were measured by means of a digital microscope Keyence VHX-500F (Keyence Corp., Osaka, Japan), shown in Figure 3.11. After measuring the diameters of the wear craters, the wear rate k_C was determined using the Eq 1.

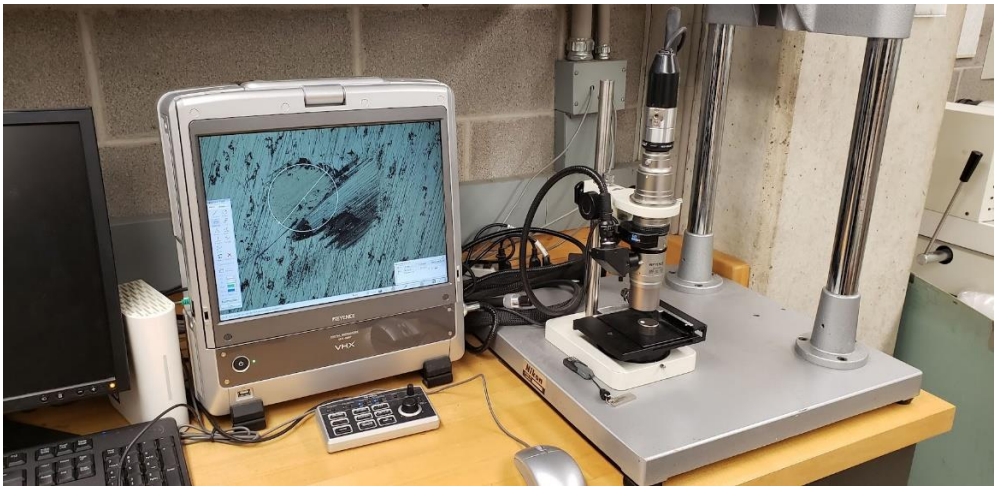

Figure 3.11. Digital microscope Keyence VHX-500F.

3.5.2 Pin-on-Disk Experiments

The tribological properties of the Nickel (Ni) and Nickel Alumina (Ni-Al_2O_3) CSAM coatings were characterized by performing pin-on-disk tribological tests following the ASTM Standard G99-05 [39]. The pin-on-disk system used was developed at the University of Texas Rio Grande Valley (UTRGV), and functions by spinning the disk sample using a motor pulley system which spins the sample holder as a pin is placed over the sample surface with a fixed load creating a circular wear track as the system makes the sample holder spin. The pin-on-disk tribometer system can be seen in Figure 3.12 below.

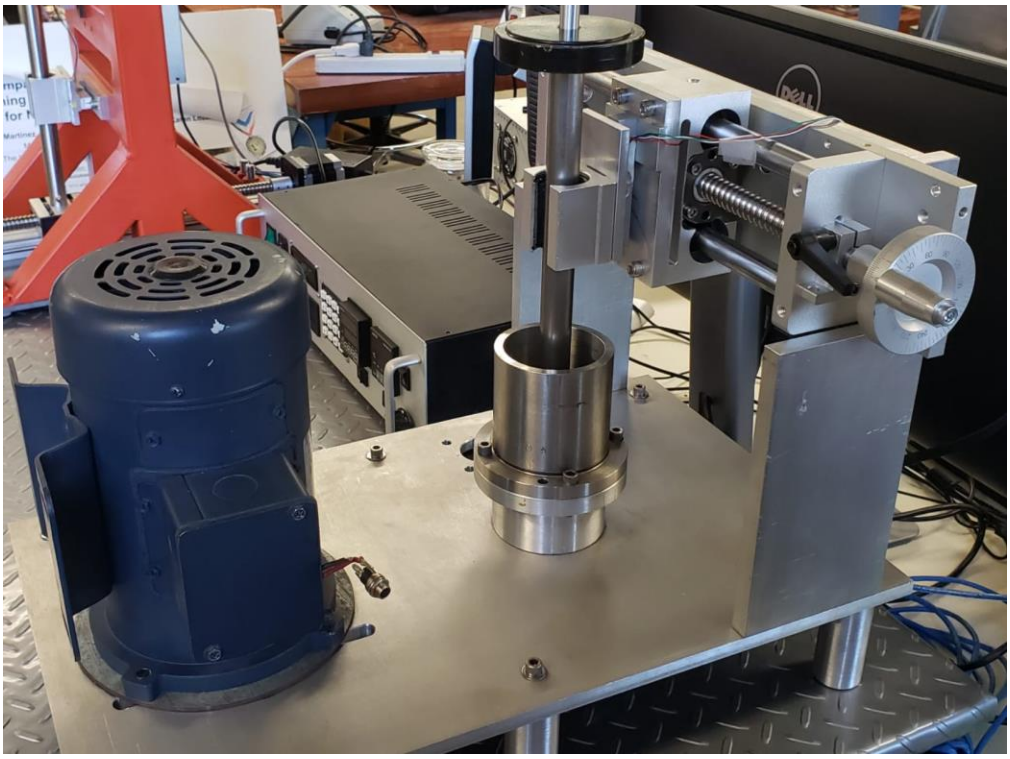

Figure 3.12. Pin-on-disk system developed at the University of Texas Rio Grande Valley.

The disk volume loss of the CSAM coatings can be determined by performing the pin-on disk tribological test using the Eq. 2, where the wear track radius of 4 mm is used, as well as the ball radius and the average wear track width which in this case was calculated by taking the wear track width measurement in 22 different areas of the wear track and calculating the average.

Eq. 2

$$\boldsymbol{disk\ volume\ loss, mm^3} = \frac{\boldsymbol{\pi} * (\boldsymbol{wear\ tack\ radius}) * (\boldsymbol{track\ width, mm})^{\boldsymbol{3}}}{\boldsymbol{6} * (\boldsymbol{sphere\ radius, mm})}$$

The calculation for the sliding distance *S*, is shown in Eq. 3 below, where *r* is the radius of the wear track scar left by the pin-on-disk experiment, *n* is the rotational speed of the sample (rpm), and *t* is the total time of the pin-on-disk experiment in minutes.

Eq.3

$$\boldsymbol{S = (2 * \pi * r)}\textbf{*(n)*(t)}$$

The friction and wear tests were carried out using the tribometer with a ball-on-disk configuration under dry conditions Each sample was tested using a 10 mm-diameter AISI 52100 bearing steel ball using the following parameters: load 5 N, sliding speed of 0.05 m/s (119 rpm), radius of circular wear tracks 4 mm, and a total sliding distance of 100 m. An uncoated Al6061 disk was tested for comparison. The coefficient of friction was continuously recorded during each test. The wear tracks on the worn specimen were analyzed by optical microscopy, SEM and EDS.

CHAPTER IV

RESULTS AND DISCUSSION

In this chapter, the experimental results of the Cold Spray research project will be presented and described in detail. It will include the CSAM coatings SEM observations describing the morphology and thickness of the coatings as well as their chemical composition. In addition, the CSAM coatings' mechanical properties will be analyzed from the roughness and microhardness results. Additionally, the tribological characteristics of the coatings will be described and analyzed from the micro-abrasion and pin-on-disk experiments. These tribological characteristics will include the determination of the wear coefficients for each coating and the coatings' thickness, determined by the calotest method. In addition, the coatings' coefficient of friction and the volumetric wear loss will be analyzed from pin-on-disk wear test results. All the results will be compared and discussed with the state-of-the-art literature on this topic.

4.1 Coating Surface Analysis

The coatings are made from Nickel (Ni) and Nickel Alumina (Ni-Al_2O_3) from (SST, Centerline, Ontario, Canada) were used to coat the aluminum 6061 disk and block samples. These coatings had the surface morphology, surface bonding, cross section and powder particles analyzed, to allow for the characterization of the CSAM coatings. These characterization tests also provided important information regarding the difference that adding alumina ceramic reinforcement does to the mechanical properties of the CSAM coatings.

When characterizing the nickel-based coatings, the first thing that was done was observing the coated samples with the visual analysis and making observations about the physical characteristics of the coatings. Figure 4.1 shows the nickel and nickel alumina block samples as they can be seen by simple visual observation. These initial observations were helpful in concluding what occurred during deposition and can help with later SEM and EDS analysis of the coating morphology, and cross-sectional analysis. As can be seen in Figure 4.1, the coated block samples for both the pure Ni (Nickel) and the Ni-Al_2O_3 (Nickel-Alumina) were placed side by side for comparison. According to (W.Y. Li et al.) the porosity was reduced because of the addition of alumina to the powder mixture. The pure nickel sample seen on the left side is riddled with small pores evenly distributed through the surface along with small circular craters. In the nickel-alumina sample seen in Figure 4.1 on the right, the coating surface color is darker than the pure nickel coating due to the addition of the alumina particles. The surface has very few pores and has few albeit large circular craters which are not evenly distributed throughout the surface.

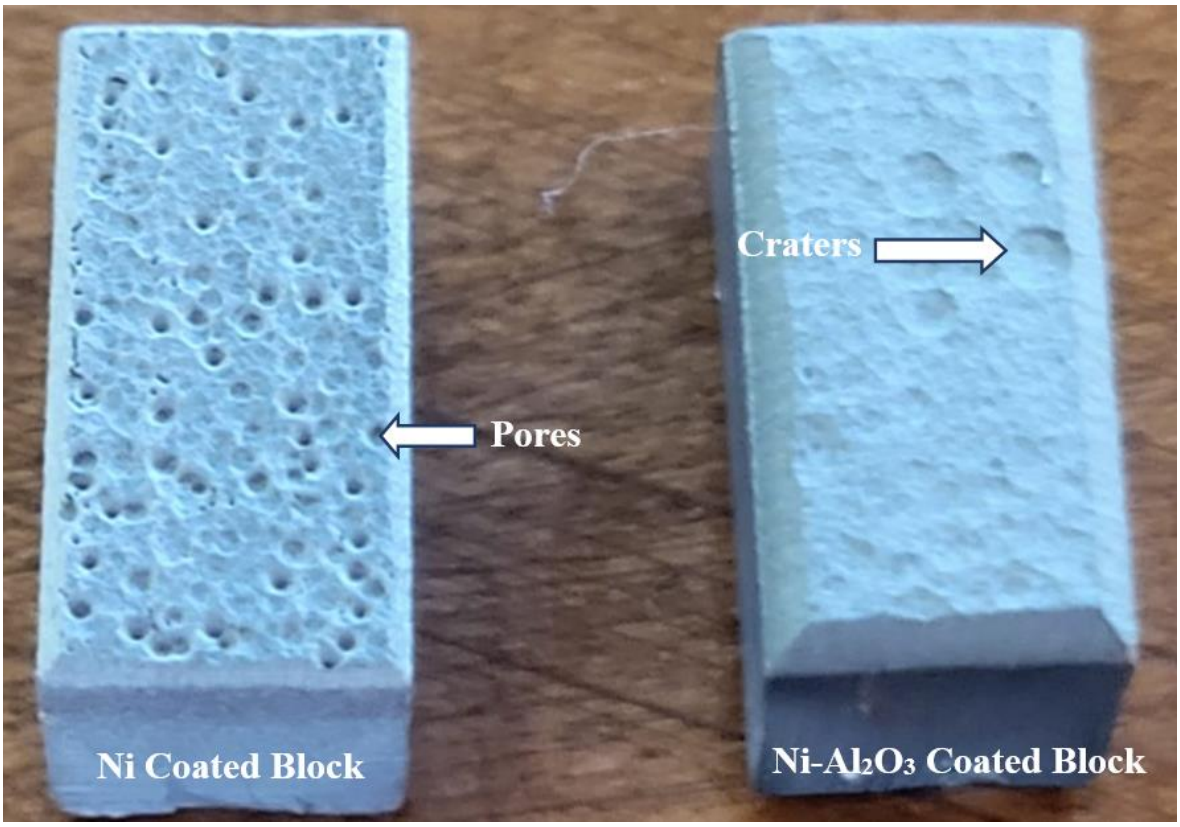

Figure 4.1. Side by side comparisons of pure Ni (Nickel) (*left*), and Ni-Al_2O_3 (Nickel-Alumina) (*right*), coated block samples.

As seen in Figure 4.2, there is a clear difference between the nickel samples and the nickel-alumina samples when analyzing the surface morphology. In the pure nickel sample in Figure 4.2a, the surface has large cracks with deep pores which is due to there being no reinforcement ceramic particles to further compress the deposited nickel powder particles. In the nickel-alumina sample seen in Figure 4.2b, there is no visible cracking on the surface with large and relatively shallow pores which are less common than in the pure nickel sample. The pores in the nickel-alumina sample are most likely caused due to the detachment of alumina particles during deposition as well as the rapid heating and cooling after deposition [33]. Since the alumina ceramic particles do not undergo semi-melting due to the high temperature of the cold spray, they do not undergo plastic deformation as they impact the surface. The hard ceramic

particles that do manage to become lodged into the CSAM coating create a shot peening effect and help reinforce the CSAM coating allowing it to have improved mechanical properties. In the Table 4.1, the manufacturer material specifications are shown with the average particle size for the powders used as well as their percent composition purity. These specifications helped understand the deposition and bonding of the CSAM deposited material onto the polished aluminum 6061 substrate.

Table 4. 1:

Coating Characteristics

Material	Composition	Particle Sizes (μm)
Ni Powder (CP-Ni)	Ni. 99.7% Min.	0.5-45 $\pm$5
Ni-Al_2O_3 MMC Mixture	Ni. 99.7% Min., Al_2O_3 92.0% Min.	0.5-45 $\pm$5

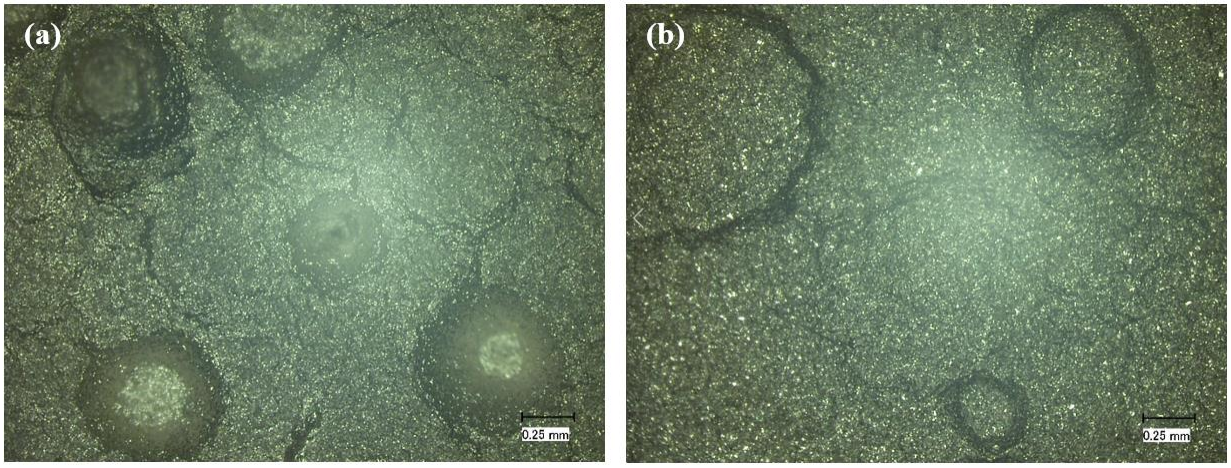

Figure 4.2. Coating morphology at 100X magnification of: (a) Ni coating and (b) Ni-Al_2O_3 metal matrix composite coating.

4.1.1 SEM (Scanning Electron Microscopy) and EDS

The samples were analyzed using a SEM (FE-SEM) ZEISS SIGMA VP system which was used to determine the average size of the particles, as well as any defects in the powder such

as smaller particles known as satellite particles. The samples were also studied with the EDS technique to understand the composition of the coatings.

As seen in Figure 4.3, SEM imaging of the pure Ni (Nickel) deposition powder shows that the powder particles come in a range of sizes and are not spherical as most spherical gas atomized CSAM deposition powders. The powder is made from particles ranging in size from 0.5-45 μm in size as seen in Figure 4.3. Upon closer analysis, the particles seem to be of irregular shape and with jagged edges which have a snowflake-like appearance. According to the powder supplier, the irregular size of the particles is to aid in achieving maximum deposition velocity [9]. The larger particles seem to be clusters of several other particles joined together to form a larger particle which may have occurred during the production process. After analyzing the powder SEM images, it was hypothesized that the jagged shape of the particles as well as the different variety of particle sized would help achieve better bonding between substrate and coating due to the smaller particles filling in any IPBs (Inter Particle Boundaries) formed during deposition.

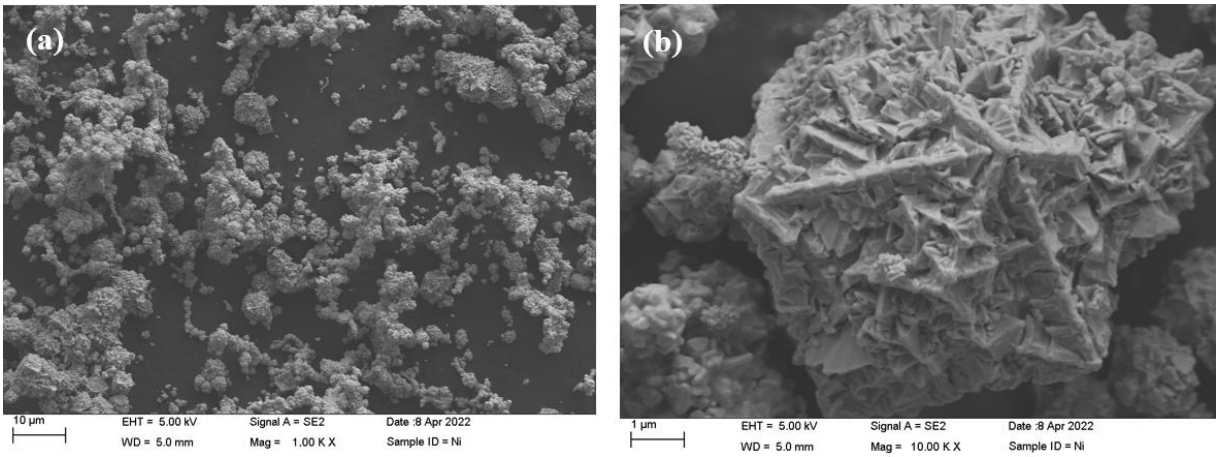

Figure 4.3. SEM images of pure Ni (Nickel) powder samples at: (a) 1000X, and (b) 10,000X magnification.

SEM images of the Ni-Al_2O_3 show the different characteristics of the alumina particles and the nickel metal matrix material, which looks identical to the material shown in Figure 4.3. As shown in Figure 4.4, there is a clear mixture of smaller nickel particles with large alumina reinforcement particles. These particles look to be much larger than the nickel particles and more solid in structure. After analyzing these images, it was hypothesized that a fair percentage of the alumina particles do not become embedded into the substrate and instead bounce off. As the alumina particles impact the surface of the substrate, they create a shot peening effect as they compact the surface of the substrate and due to the high velocity become embedded deep into the coating.

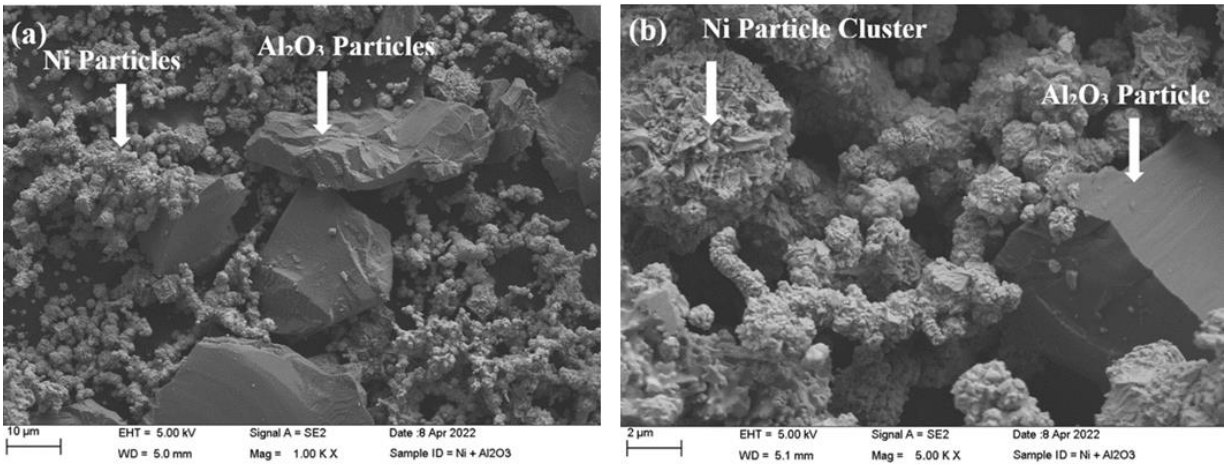

Figure 4.4. SEM images of Ni-Al_2O_3 (Nickel-Alumina) CSAM powder at: (a) 1,000X and (b) 5,000X magnification.

As seen in Figure 4.5, the cross-sectional area of the aluminum 6061 block samples can be seen where the substrate pointed out in the bottom and the coating on top of the substrate layer is bonded to the surface of the substrate. The bonding on the nickel coating seems to be different than the bonding of the nickel-alumina coating which seems to have a major crack between the substrate and coating. This cracking most likely caused during deposition as stated by (K. Spencer et al.) because of poor cohesion between the powder particles. The crack in

Figure 4.6 is most likely also due to the alumina particles bouncing off the surface during deposition [31]. The jagged surface where the coating and substrate bond together is most likely due to the deformation that occurs as the CSAM coating particles impact the soft aluminum substrate with high kinetic energy and the incorporation of hard alumina reinforcements causing deformation of the substrate surface [31]. In Figure 4.5b, the layered nickel particles can be seen where there are internal pores in between them as pointed out by the arrow. These pores are dispersed throughout the coatings and point to a limited plastic deformation upon impact and rapid cooling [33].

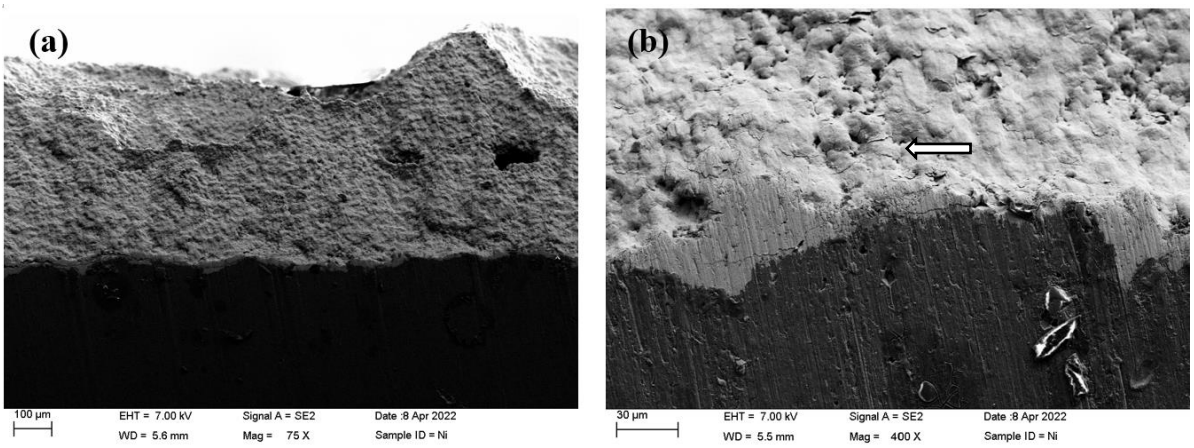

Figure 4.5. SEM image of cross-sectional area of Ni (Nickel) CSAM coating showing the coating thickness, at (a) 75X, and (b) 400X magnification.

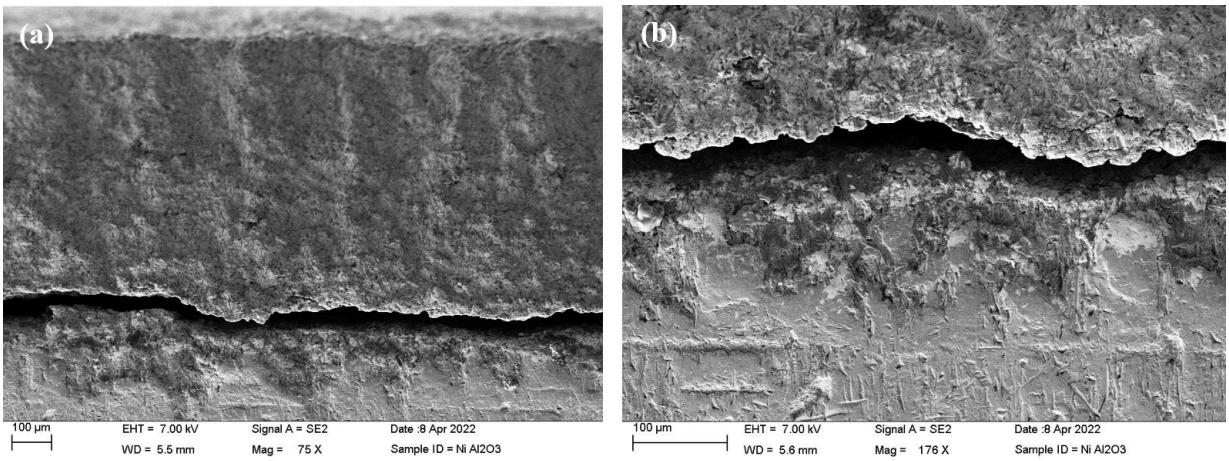

Figure 4.6. SEM images of cross-sectional area of Ni-Al_2O_3 (Nickel-Alumina) coated block sample at (a) 75X, and (b) 176X magnification.

An EDS analysis was performed on the nickel-alumina powder mixture to analyze the elemental composition of the powder mixture and confirm that the CSAM powder was in fact a pure nickel mixture with alumina particles and to ensure that the identification of the individual particles was correct. Two areas were selected to be analyzed by EDS technique as can be seen in Figure 4.7. The Area 1 selected was an area on a flat face of one of the alumina particles seen mixed in with the nickel particles. This was chosen because there seems to be a solid flat face with no contamination which would give us a highly accurate result as to the composition of the selected material. The Area 2 was selected to be on a large cluster of nickel powder particles in order to be sure to get accurate results. The results of both the selected areas are shown below in Figure 4.8, where the selected Area 1, shows two large peaks which were expected as the first one detects oxygen and the second detected aluminum. These results were as expected as alumina is comprised of oxidized aluminum material. The results for the second selected area showed a large peak for pure nickel material, as well as two smaller peaks of oxygen and carbon. The presence of carbon is to be expected as carbon is abundant in the earth and can be found everywhere.

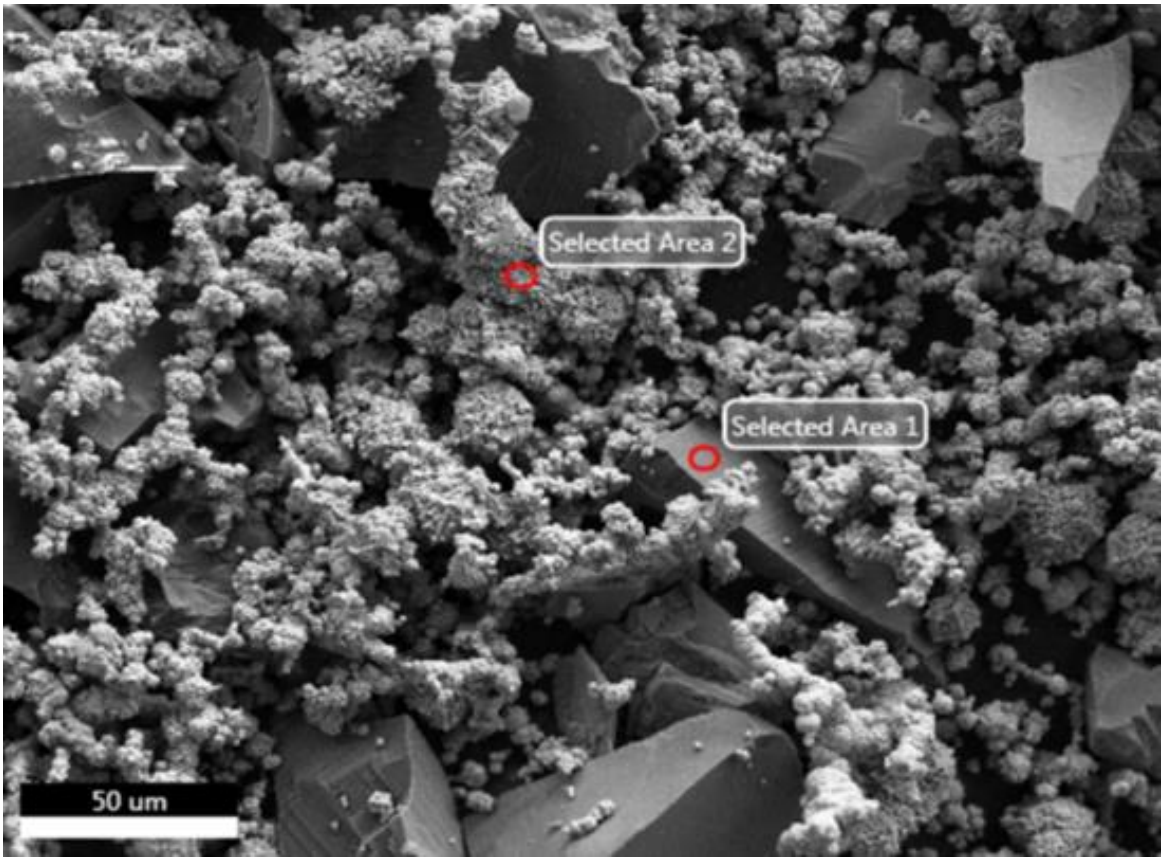

Figure 4.7. Ni-Al_2O_3 (Nickel-Alumina) powder sample selected EDS analysis areas.

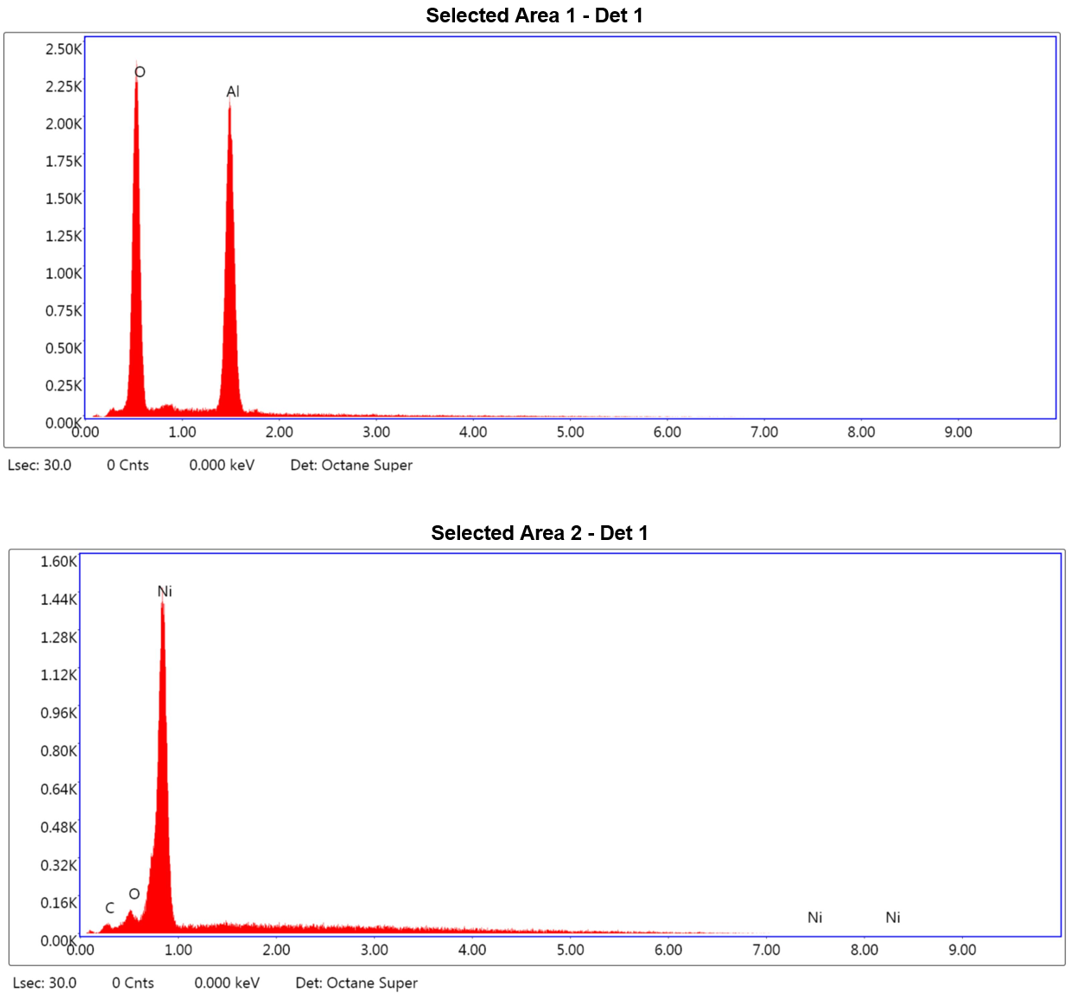

Figure 4.8. EDS results of selected Areas 1 and 2 elemental composition results.

4.1.2 Microhardness

Microhardness was tested at a load of 200g at different points which were laid out vertically as seen in Figure 4.9b. The layout was intentionally done to be able to find the indentations a lot easier. Each sample was subjected to different iterations so as to take an average microhardness value for each sample tested. The microhardness values were as expected, and the side-by-side comparison of the Vickers hardness values can be seen in Figure 4.7. where they are compared to each other. The results show that the addition of alumina to the

nickel deposition material was effective in increasing the density and thus the surface hardness of the CSAM coating.

In Figure 4.9, the Vickers hardness indentations for the aluminum 6061 and the nickel and nickel-alumina coated samples can be seen. The indentation for the uncoated aluminum 6061 sample yielded the larger indentation, thus generating a lower Vickers hardness value as expected. The nickel and nickel-alumina coated samples had nearly identical pyramidal indentations with little variation in size, with the nickel-alumina samples being slightly larger resulting in a slightly lower Vickers hardness value.

The hardness results can be seen in Figure 4.10, with the obviously lower Vickers hardness value for the uncoated aluminum 6061 sample, with results that were overall consistent in the 5 different iterations taken. As can be seen in Figure 4.10, the results for the Vickers hardness of both the coated samples resulted in very similar values, with the pure nickel coated sample having a slightly higher hardness value. This may have occurred due to the large alumina particles bouncing off of the surface and not adhering correctly to the surface, resulting in a coating with a slightly lower hardness.

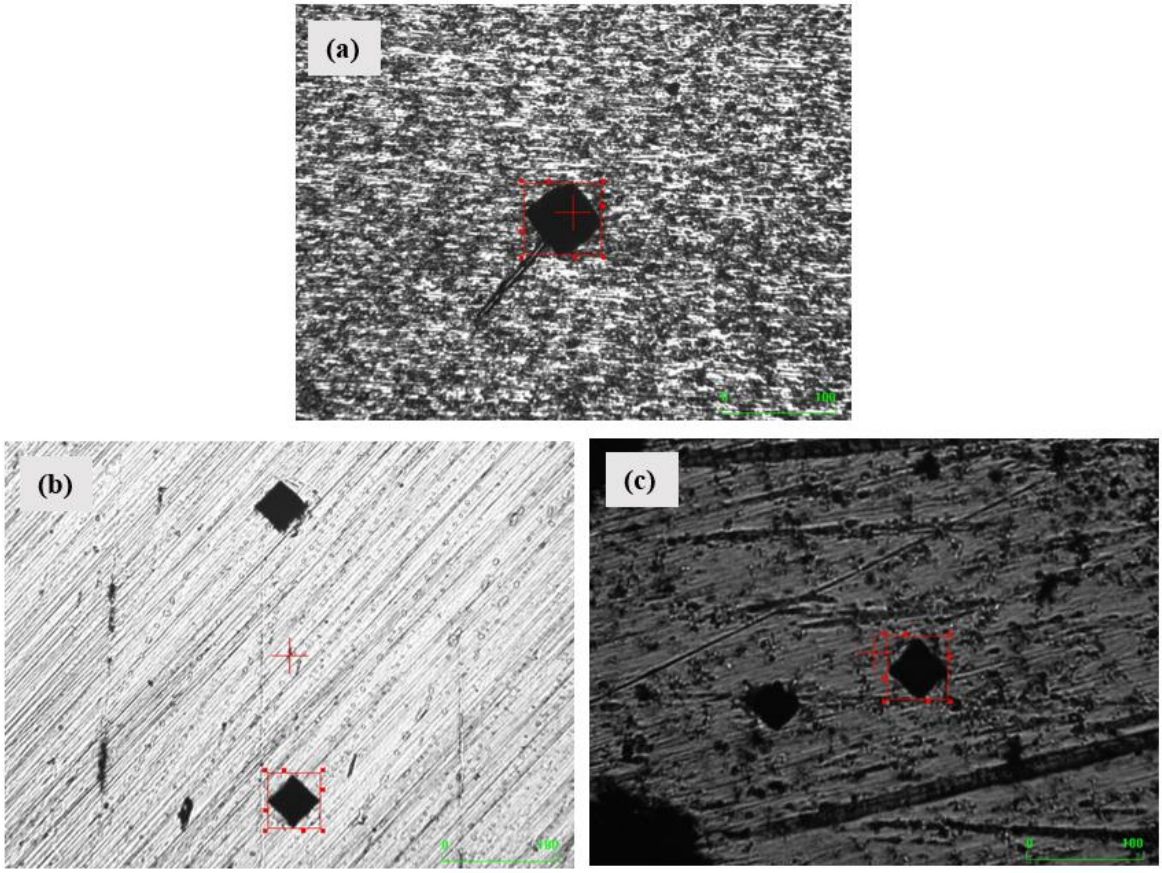

Figure 4.9. Vickers Hardness pyramidal indentations of the (a) Aluminum 6061 uncoated sample, (b) Nickel coated sample (c) Nickel-Alumina coated sample.

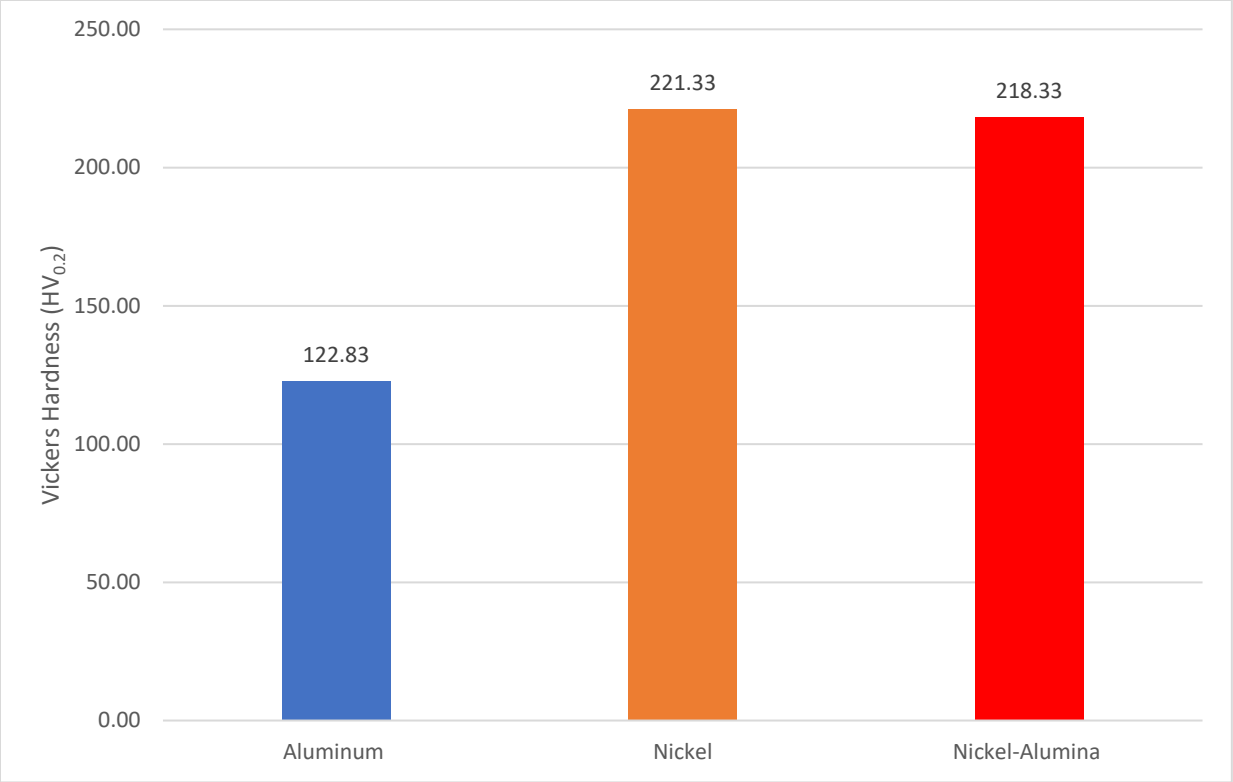

Figure 4.10. Microhardness measurements.

In other studies, done on testing the Vickers hardness of CSAM coatings with a pure single material metal coating versus one with a metal matrix base material, reinforced with ceramic particles, the results consistently showed that for pure Al and for an alumina reinforced aluminum CSAM MMC coating, the increase in microhardness was noticeable but not significant because of the addition of reinforcement alumina particles [31]. According to W. Y Li et al., who investigated CSAM coatings made from Ni-Al_2O_3 the bulk nickel and nickel alumina coatings performed better than the uncoated sample. The results from W. Y. Li et al. for a nickel-alumina coating in an Inconel 600 substrate yielded a hardness value of 206 Hv which is lower than what can be seen in in Figure 4.10. This may be due to the particle sizes used in the study by W. Y. Li et al. of about 85 μm which is much larger than the 0.5-45 μm powder size used in this study. The CSAM coating deposition technique also differed as the deposition standoff distance was 30 mm [33] while the standoff distance used in this study was 12 mm.

4.2 Tribological Characterization

4.2.1 Micro-Abrasion Tests

To determine the wear resistance of the nickel based CSAM coatings, micro-abrasion calotte tests were performed with the Anton Paar Compact CAT2c Calotester (Anton Paar GmbH, Graz, Austria) which used a 30 mm diameter steel rotating ball to create a wear track on the surface of the coated disk. The analysis of the wear scars was performed by the Keyence VHX-500F digital microscope.

The micro-abrasion wear scars are a circular wear-scar created by the rotating calotest steel ball spinning on the surface of the sample. In Figure 4.11, the wear scars for both the pure nickel coated disk sample as well as the nickel alumina disk sample are shown. After analyzing the wear scars left on both samples under an optical microscope, it was obvious that there were fine grooves in the up-down direction left by the calotest ball. The wear scars left by the tests that had a higher number of revolutions were more clearly defined, especially around the edges of the wear scar. This can be seen as in Figure 4.12a and Figure 4.12d which had longer sliding distances show more defines wear scars. As the samples were porous, polishing the surface did little to rid the surface of pores, in some cases such as seen in Figure 4.11a, the pores in the coating interfered with the calotest affecting the wear scar measurements. The pores created during the CSAM deposition created a dense area surrounding the porous craters as particles were compacted by the crater. This effect can be seen in the upper left-hand corner of the wear scar on Figure 4.11a, where the area surrounding that small crater was unaffected by the calotest.

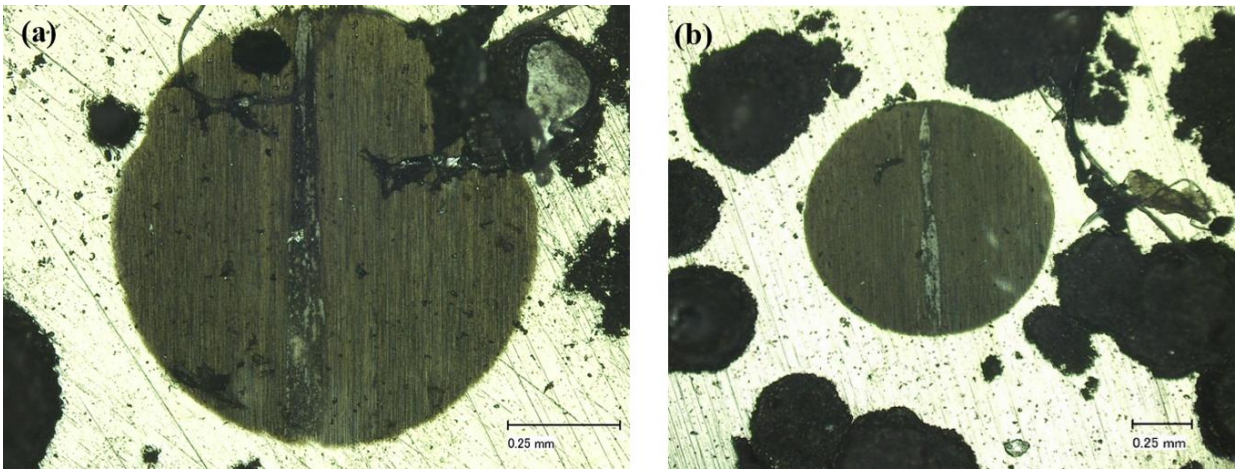

Figure 4.11. Micrographs of the concave wear scars produced by the rotating steel ball on the Nickel coated aluminum 6061 disk at (a) 200X, and (b) 100X magnification.

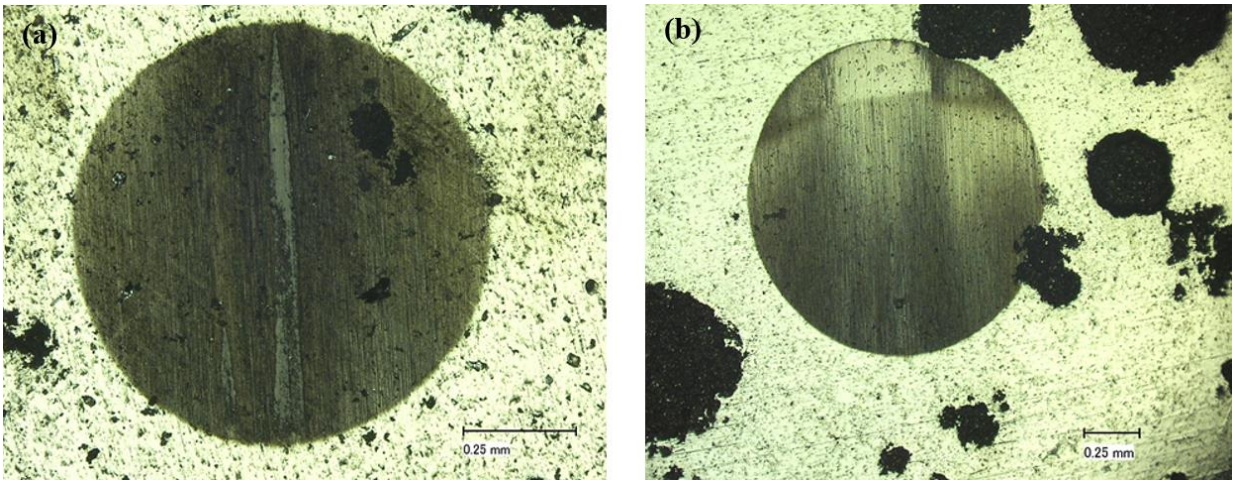

Figure 4.12. Micrographs of the concave wear scars produced by the rotating steel ball on Nickel-Alumina coated aluminum 6061 disk sample (a) 200X, and (b) 100X magnification.

After calculating the wear rates of the nickel and nickel-alumina coated material as well as of the bulk substrate aluminum 6061 material as seen on Table 4.2, the results were unexpected as the nickel-alumina coating had slightly higher wear than the pure nickel coated sample. This was unexpected as it was common to see in similar studies [33] that the addition of ceramic reinforcement particles helped enhance the tribological properties of the coating. This however was not the case as the pure nickel coating had a slightly better coefficient of friction. The conclusion reached after analyzing the nickel-alumina powder and the wear scars shown in

Figure 4.13 is that most likely the breaking off of the larger alumina particles embedded in the relatively smaller nickel particles caused the nickel-alumina sample to experience higher wear resulting in a higher wear rate.

Table 4.2. Micro-abrasion coefficient of Friction for Aluminum 6061, (Ni) Nickel and Ni-Al_2O_3 (Nickel-Alumina)

Sample	k_c x 10^{-13} (m^3/mN)	k_s x 10^{-13} (m^3/mN)
Aluminum 6061	-	3.31
Ni (Nickel)	1.40	-
Ni-Al_2O_3 (Nickel Alumina)	1.51	-

4.2.2 Pin-on-Disk Tribological Experiment Results

The pin-on-disk tests were done on an in-house designed and built pin-on-disk tribometer system (The University of Texas Rio Grande Valley, USA). The pin-on-disk system was set to run at a rotating speed of 119 RPM with a normal load of 5 N acting downward on the sample. The pin is made from AISI 52100 bearing steel with a 10 mm diameter. When analyzing the wear track left by the pin-on-disk testing, the wear track left on the pure nickel coated sample was much more uniform despite the higher number of craters on the surface.

As seen in the Figure 4.13, the Digital microscope Keyence VHX-500F images of the wear tracks for the nickel and nickel-alumina coated disk samples are shown below. The physical appearance of the two wear tracks left by pin-on-disk tribological experiments is very different upon initial analysis. The pure nickel coating wear track appears to be much more clearly defined with the edges being more clearly defined. The average wear track width taken after calculating the average of 22 measurements of the wear scar width gave an average width of 0.641 mm as seen in Figure 4.13. This wear track with the high level of uniformity and clearly

defined borders is due to the pure nickel coating being of a single homogeneous material with the same material properties throughout. The different ranges of particle size suggest that during deposition, the smaller particles were able to fill in porous areas in the coating and this created a coating with consistent density.

When analyzing the wear scar for the nickel-alumina coated sample in Figure 4.13c, the digital microscope image was surprising as the wear scar had rough edges and inconsistent wear width diameters. The border of the wear scar was not clearly defined as seen in the nickel coated wear scar in Figure 4.13a and Figure 4.13b. There was also a different colored material not seen in the pure nickel wear scar that had a different reflection when under the microscope. It was hypothesized that the jagged profile of the wear scar was due to the fact that this coating had a significant percentage of alumina added to it, and this was a result of the much larger alumina particles becoming loose during the pin-on-disk experiment and this resulted in the loss of a greater amount of material. This loss of material is evident in Figure 4.13 as the nickel-alumina coating had a slightly higher average wear scar width compared to the nickel coated sample wear scar.

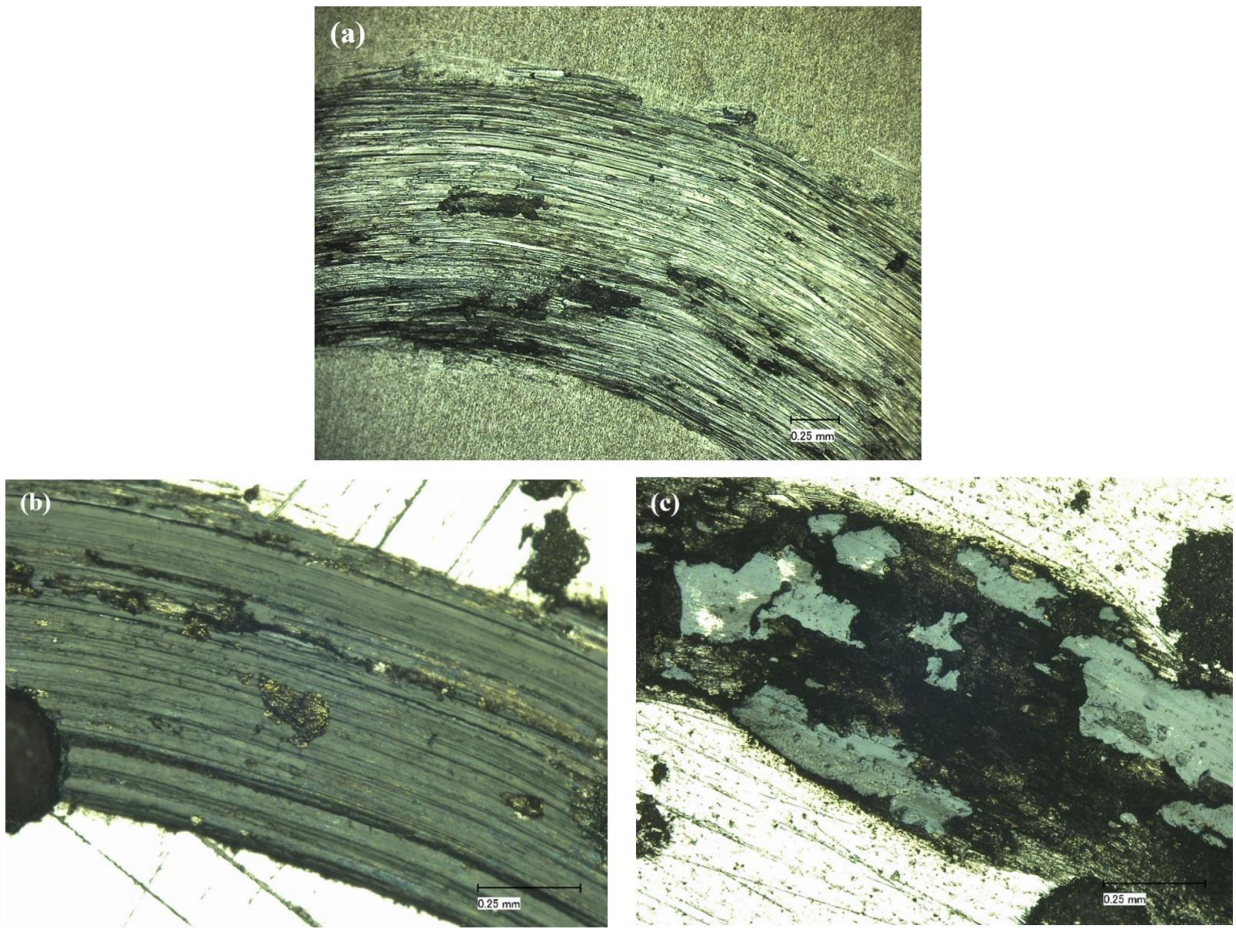

Figure 4.13. Micrographs of the wear tracks left on the (a) Al6061 specimen without coating at 100X, (b) nickel coated and (c) nickel-alumina coated disk samples at Magnification 200X.

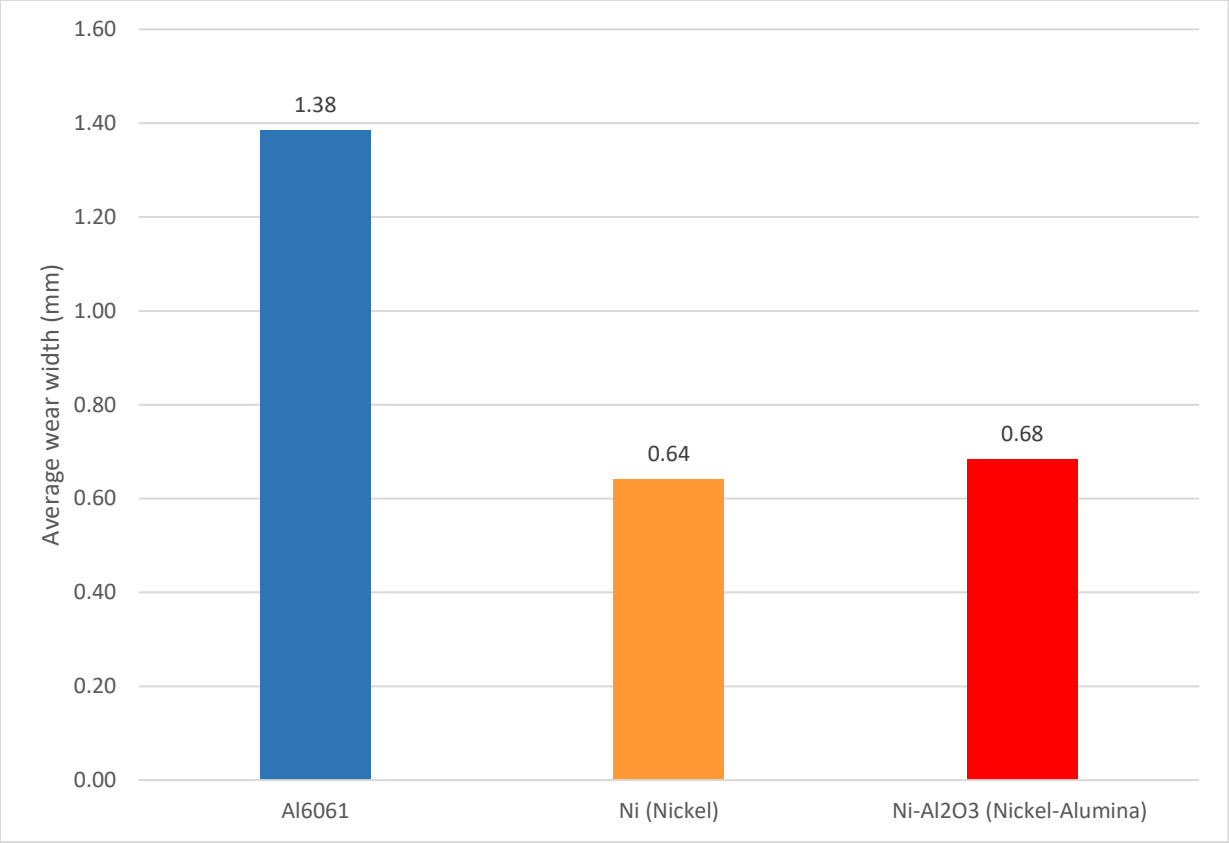

Figure 4.14. Pin-on-disk average wear scar width values (mm) calculated by taking 22 measurements throughout the wear scar.

By using the calculated wear track width values for the aluminum 6061 uncoated sample, as well as the nickel and nickel-alumina samples, the wear rate was able to be calculated using the ASTM G99 International Standard for Pin-on-disk testing [39]. The results were surprising as the nickel-alumina samples had a higher wear rate than the pure nickel coating as is evident in the side-by-side comparisons of this data seen in Figure 4.15. This was different to the initial hypothesis that the nickel-alumina would result in a lower wear rate compared to the sample with no alumina content. This however was proven incorrect because it was not taken into consideration that the powder material that would be used in these experiments would not be spherical gas atomized metal particles, nut instead the particles were of varying sized and seem to be crushed up and are not of consistent shape. The alumina particles are also much larger than

individual nickel particles, resulting in the alumina particles contributing to higher volumetric wear loss as they broke off during the pin-on-disk experiments. It is evident however that the hard nickel-alumina coating was of high quality as it was able to wear away material from the AISI 52100 bearing steel pin where the pure-nickel coating did not.

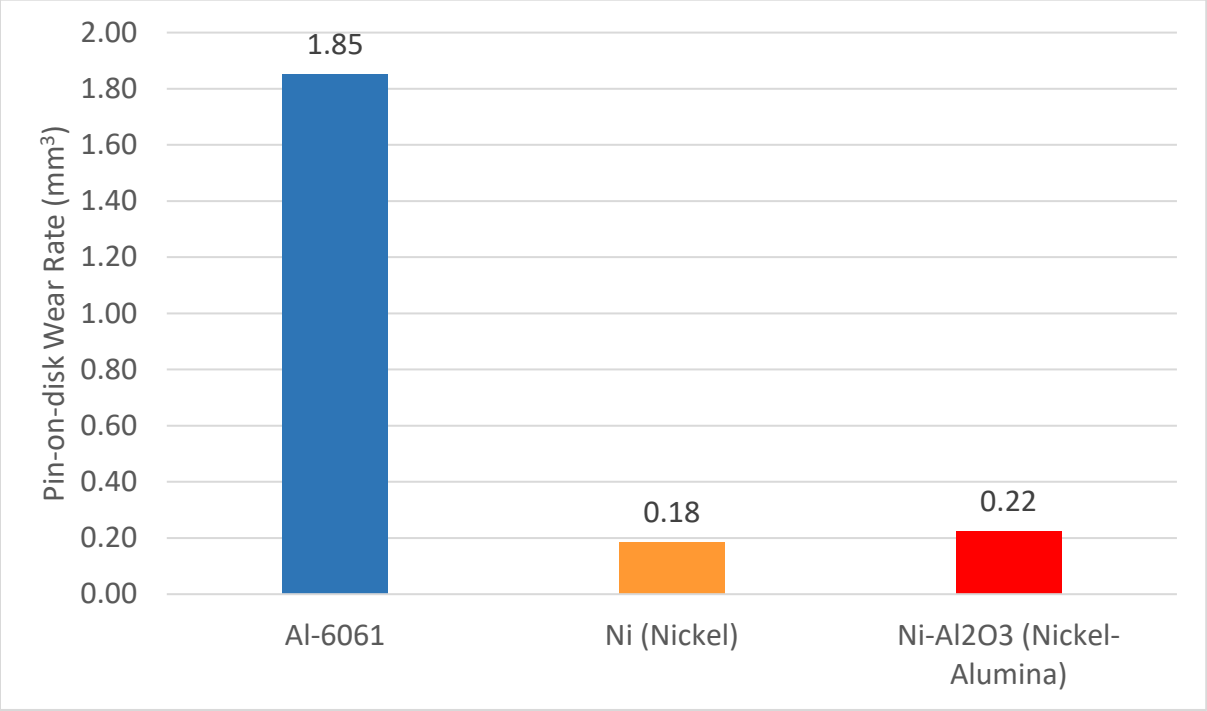

Figure 4.15. Mean volumetric wear of CSAM coated disks tested against AISI 52100 steel balls.

After observing the presence of a possibly different material under the digital microscope images of the wear scar for the nickel-alumina coating seen in Figure 4.13, an EDS content analysis was performed on the wear scar as shown in Figure 4.16. It was hypothesized after seeing the Image on Figure 4.13c, that the unknown material adhered on the wear scar with a different shining profile was material that was adhered to the nickel-alumina coating from the AISI 52100 bearing steel pin used in the pin-on-disk experiments. Due to the nickel-alumina coating being more wear resistant than the AISI 52100 bearing steel pin, the material worn out form the pin was adhered to the surface of the nickel-alumina wear scar. To confirm this

hypothesis, the EDS content analysis test were performed, and three areas were selected as seen in Figure 4.16, to understand the contents of what was seen under the digital microscope image seen on Figure 4.13. The first selected area was what looked to be a convex deposited material patch in the middle section of the wear scar, which would be the different colored material seen in Figure 4.13. The second selected area was also in the wear scar and was hypothesized to be the nickel-alumina coating. The final selected area for analysis was a flat area outside of the wear scar to have a reference as to what the coating on its own is made from, making it easier to identify any new elements present after the pin-on-disk testing.

The results of the EDS analysis confirmed the initial hypothesis made to be correct, as the data results in Figure 4.17 show. In the results for the first selected area, had as predicted, a high nickel content present, however the hypothesis made was proven correct as there was also a significant amount of iron found in that area as well as a high amount of carbon, which makes up a significant portion of the AISI 52100 bearing steel pin used in the pin-on-disk tribological experiments. These results confirm that there was adhesive wear as material from the AISI 52100 bearing steel ball adhered to the surface of the nickel-alumina coating. The significant amount of oxygen detected by the EDS test also sheds light on tribo-oxidation that occurs when there is oxidation on the metal caused by the wear temperature and friction during the tribological test. This presence of oxygen was also seen significantly in the selected Area 2, which had significantly less iron content, and an even lower nickel content which means that the area inside the wear track was left with less nickel and the tribological test ended up adding new material to the wear track surface and the conditions of loading and friction caused a chemical reaction resulting in tribo-oxidation occurring.

In the Area 3 of the EDS test, which was outside of the wear track, the expected results were shown as there was a high concentration of nickel and trace amounts of oxygen and carbon which are commonly found in nature. The results of the selected Area 3 are confirmed as they are nearly identical to the results in the selected Area 2 of Figure 4.7 mentioned previously, which was an analysis of the nickel-alumina powder.

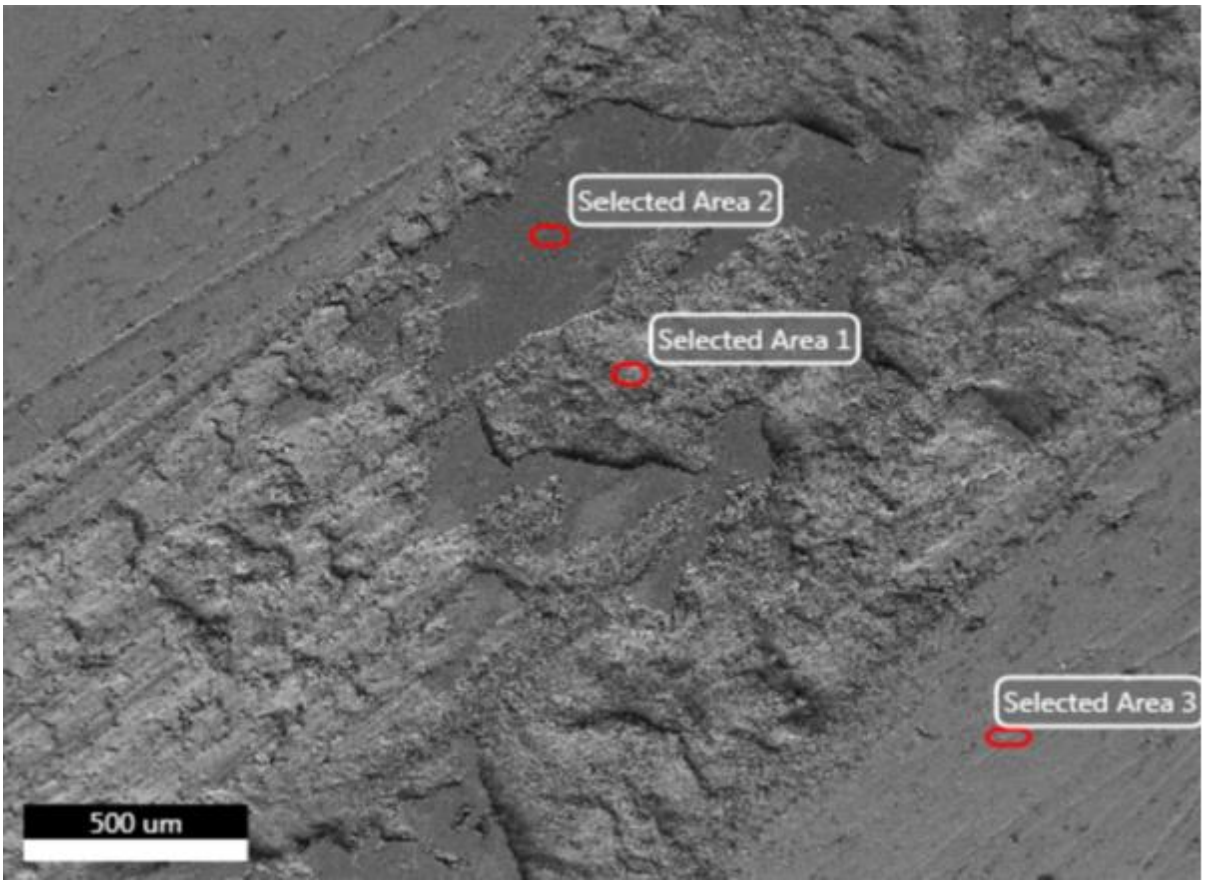

Figure 4.16. Ni-Al_2O_3 (Nickel-Alumina) wear track selected areas for EDS analysis.

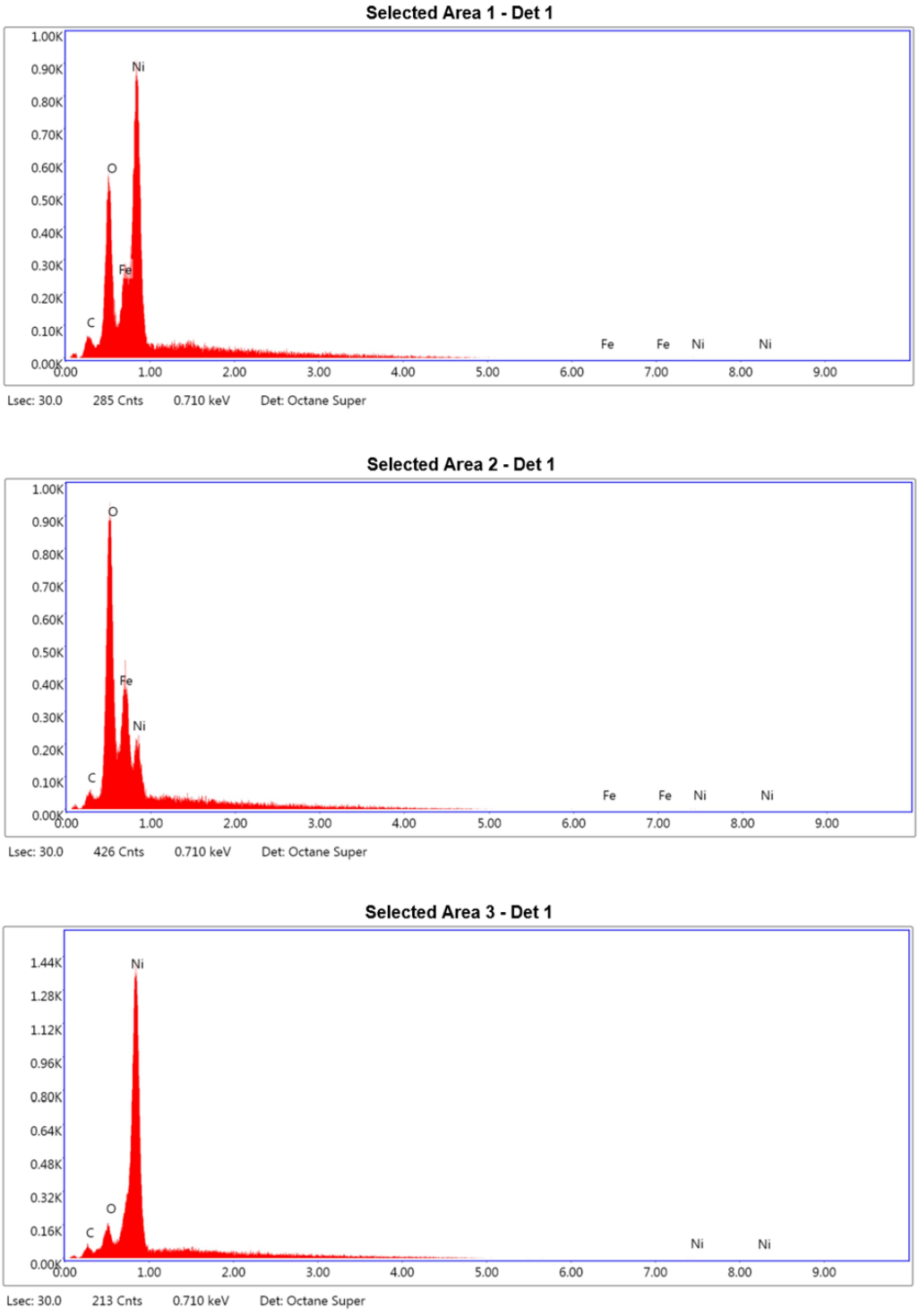

Figure 4.17. SEM analysis results for the three selected sections.

The pin-on-disk experiments yielded the coefficient of friction of the nickel and nickel-alumina samples as well as an aluminum 6061 bulk alloy sample which was tested as a reference. The

results are shown in Figure 4.18 which show the coefficient of friction versus the sliding distance up to 100 meters, after which there is a plateau in the results as they reach steady state. For all three plots, there is characteristic immediate jump in coefficient of friction that goes up to about a sliding distance of 10-20 m, after which the plots all seem to reach the steady state. The most significant jump in coefficient of friction is seen in the nickel alumina plot shown in Figure 4.18 in red, where before the sliding distance reaches 10 meters, there is a jump which reaches to a coefficient of friction just below 0.9. After the 10 m sliding distance, the coefficient of friction drops to steady state of about 0.6-0.65 coefficient of friction. This major jump is due to there being resistance to wear in the initial stages of the pin-on-disk test, after which it reaches steady state when the wear scar is established.

The nickel sample has the lowest peak of initial coefficient of friction as at its highest peak, it reached just below a 0.6 value of coefficient of friction, before dropping to a steady state coefficient of friction of about 0.3. This is due to the homogeneous condition of the pure nickel CSAM coating which allows for there to be less friction compared to the nickel-alumina coating which has a higher coefficient of friction due to the alumina particles creating higher friction.

The bulk aluminum 6061 uncoated sample shows a slightly different plot profile, as there is an initial jump in coefficient of friction, however there is not an abrupt drop to steady state, as the plot shows that after the aluminum coefficient of friction plot reaches the peak of just below 0.6, after which it goes into a steady decline and does not reach steady state until it gets to a sliding distance of about 50 meters. This can be explained because aluminum 6061 is a much softer material than nickel and nickel alumina, therefore the pin becomes bogged down in the softer material compared to the pin sliding easily on the harder nickel-based coatings. The plot

shows that the aluminum 6061 material reaches a coefficient of friction of about 0.25 at steady state, just slightly lower than the pure nickel sample.

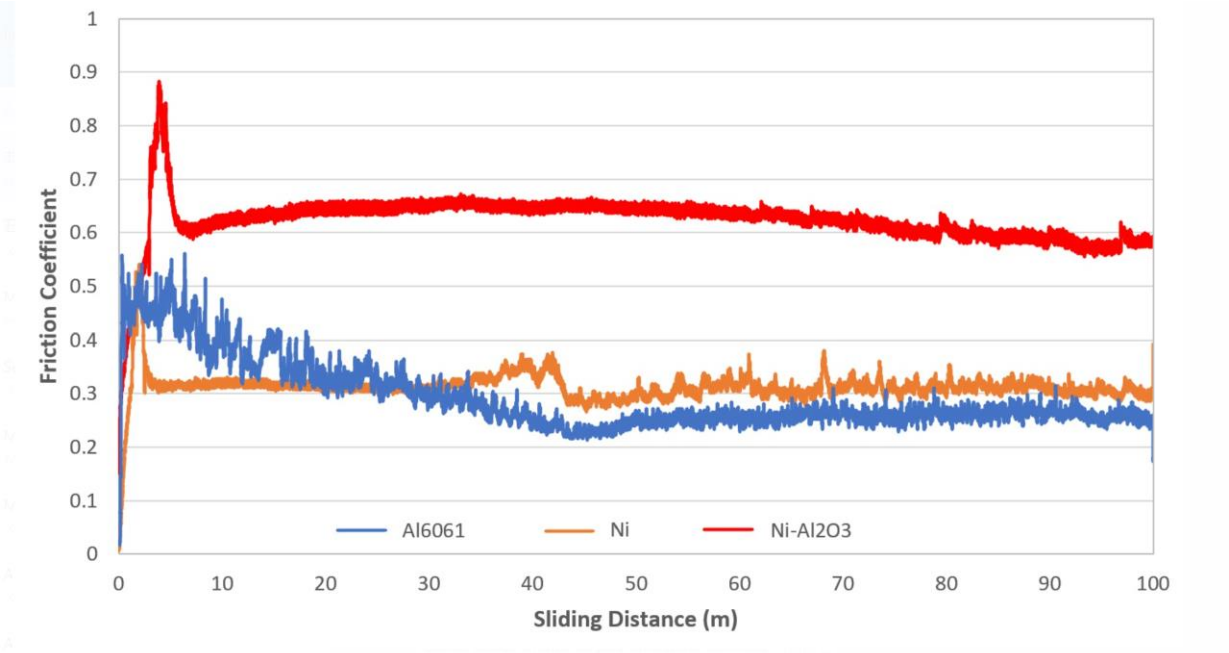

Figure 4.18. Friction coefficient vs. sliding wear distance during pin-on-disk experiments.

CHAPTER V

CONCLUSION

In the present research project, the effect of Al_2O_3 additions on the tribological properties of nickel cold spray coatings deposited on aluminum specimens were investigated. The coatings were characterized utilizing scanning electron microscopy, and microhardness testing. The tribological performance of the nickel cold spray coatings with and without Al_2O_3 additions was evaluated using an abrasive wear test based on the ball-crater technique. In addition, the wear and friction characteristics of the CSAM coatings were evaluated with a pin-on-disk tribometer. Based on the experimental results, the following main conclusions can be drawn:

From the microhardness measurements, it was found that the addition of the alumina particles did not have a drastic effect on microhardness, as the results showed that the pure nickel coating had a slightly higher hardness. This can be attributed to the differences between the nickel particles and the larger more solid structured Al_2O_3 particles which may have not adhered evenly on the coating and caused soft spots in the coating surface.

In this research project, the addition of Al_2O_3 particles was studied and the changes it had to the mechanical and tribological properties were evaluated. Moreover, it was found that the addition of Al_2O_3 particles did not help the tribological properties of the coating, with these

actually being slightly more susceptive to wear, the addition of alumina particles to the CSAM coating was highly effective in decreasing porosity in the coating. The results of the characterization of the nickel-alumina coating suggest that the addition of alumina particles helped to improve surface quality of the coated surface, without compromising on many of the enhanced mechanical and tribological properties that nickel-based CSAM coatings have to offer.

When performing a tribological evaluation on the coatings which included the calotest and the pin-on-disk wear test, the Al_2O_3 infused coating performed slightly poorer than the pure nickel coating. The wear coefficient and wear rates calculated by the calotest, and pin-on-disk tests respectively showed results in which the pure nickel coating performed slightly better than the $AlO3$ particle infused coatings. These results were validated by the microhardness tests which showed the pure nickel coating performing only slightly better than the Al_2O_3 particle infused coating. These results are likely because during wear testing, the larger $AlO3$ particles became dislodged from the surface of the coatings leaving the surface with empty spaces where the alumina particles were embedded in the coating. This loss of large Al_2O_3 particles contributed to the slightly higher wear rates and wear coefficient.

EDS technique results and digital microscope imaging of the nickel-alumina coating pin-on-disk wear track confirmed the presence of material from the AISI 52100 bearing steel ball used in the pin-on-disk was found adhered to the surface. This indicated that there was cold welding occurring during the pin-on-disk experiment.

The research results proved that the CSAM nickel-based coatings greatly improved the tribological properties of the aluminum 6061 material, as the pin-on-disk wear rate showed that the coated samples had an average of about 90% decrease in wear due to the CSAM coatings. The coefficient of friction for the nickel and nickel alumina coated samples showed an average of 36%

better coefficient of friction compared to the uncoated aluminum 6061 sample. These improvements in results indicate the addition of nickel based CSAM coatings was highly effective in improving the overall tribological properties of the aluminum 6061 material.

In summary, it was found that cold spray coatings can increase the working life of a component and help diminish the tribological effects of wear due to friction by creating a highly dense outer coating on the surface of the substrate. In addition, cold spray can be used in different coating applications with a wide range of different metals and alloys. CSAM coatings have an unlimited range in applications where rapid repair and high-quality coatings are needed. The ease of use of this technology has a promising future in aerospace and defense applications as it provides a low-cost solution for corrosion prevention and repair of damaged components.

CHAPTER VI

FUTURE WORK

- In the future, CSAM coatings will be developed in the UTRGV engineering laboratories and will be tested for mechanical and tribological properties, as well as anti-corrosion protective properties.
- The development of components with complex geometries will also be studied and developed with a low-pressure cold spray system.
- The effects of temperature, pressure and spray distance and method will be optimized for higher quality deposition of metal feedstock powder.

REFERENCES

[1] Widener, C. A., Carter, M. J., Ozdemir, O. C., Hrabe, R. H., Hoiland, B., Stamey, T. E., Champagne, V. K., & Eden, T. J. (2015). Application of High-Pressure Cold Spray for an Internal Bore Repair of a Navy Valve Actuator. *Journal of Thermal Spray Technology*, *25*(1–2), 193–201. https://doi.org/10.1007/s11666-015-0366-4

[2] Zhang, Peirong, et al. "On Machinability and Surface Integrity in Subsequent Machining of Additively-Manufactured Thick Coatings: A Review." *Journal of Manufacturing Processes*, vol. 53, 2020, pp. 123–143., doi:10.1016/j.jmapro.2020.02.013.

[3] *ООО "АПИК Технолоджи"*. Димет - оборудование для холодного напыления металлов. (n.d.). https://dimet.info/.

[4] Jadidi, M., Moghtadernejad, S., & Dolatabadi, A. (2015). A Comprehensive Review on Fluid Dynamics and Transport of Suspension/Liquid Droplets and Particles in High-Velocity Oxygen-Fuel (HVOF) Thermal Spray. *Coatings*, *5*(4), 576–645. https://doi.org/10.3390/coatings5040576

[5] Tikkanen, J., et al. "Characteristics of the Liquid Flame Spray Process." *Surface and Coatings Technology*, vol. 90, no. 3, 1997, pp. 210–216., doi:10.1016/s0257-8972(96)03153-2.

[6] Wang, J., Sun, B., Guo, Q., Nishio, M., & Ogawa, H. (2002). Wear Resistance of a Cr_3C_2-NiCr Detonation Spray Coating. *Journal of Thermal Spray Technology*, *11*(2), 261–265. https://doi.org/10.1361/105996302770348925

[7] Yin, S., Cavaliere, P., Aldwell, B., Jenkins, R., Liao, H., Li, W., & Lupoi, R. (2018). Cold spray additive manufacturing and repair: Fundamentals and applications. *Additive Manufacturing*, *21*, 628–650. https://doi.org/10.1016/j.addma.2018.04.017

[8] *equipment, powder materials and workshop*. Low Pressure Cold Spray Technology. (n.d.). http://dymet.ee/.

[9] *SST™ Powders*. CenterLine Supersonic Spray Technology. (n.d.). https://www.supersonicspray.com/products/sst-powders.

[10] Nikbakht, R., Assadi, H., & Jodoin, B. (2020). Intermetallic Phase Evolution of Cold-Sprayed Ni-Ti Composite Coatings: Influence of As-Sprayed Chemical Composition. *Journal of Thermal Spray Technology, 30*(1-2), 119-130. doi:10.1007/s11666-020-01112-8

[11] Prashar, G., & Vasudev, H. (2021). A comprehensive review on sustainable cold spray additive manufacturing: State of the art, challenges and future challenges. Journal of Cleaner Production, 310, 127606. https://doi.org/10.1016/j.jclepro.2021.127606

[12] Villafuerte, J. (2020). Commercial Cold Spray Equipment. Materials Forming, Machining and Tribology, 19–32. https://doi.org/10.1007/978-3-030-42756-6_2

[13] Gell, M., Jordan, E. H., Teicholz, M., Cetegen, B. M., Padture, N. P., Xie, L., Chen, D., Ma, X., & Roth, J. (2007). Thermal Barrier Coatings Made by the Solution Precursor Plasma Spray Process. Journal of Thermal Spray Technology, 17(1), 124–135. https://doi.org/10.1007/s11666-007-9141-5

[14] Schiller, G., Henne, R., & Borck, V. (1995). Vacuum plasma spraying of high-performance electrodes for alkaline water electrolysis. Journal of Thermal Spray Technology, 4(2), 185–194. https://doi.org/10.1007/bf02646111

[15] Nasif, G., Barron, R. M., Balachandar, R., & Villafuerte, J. (2019). Numerical assessment of miniaturized cold spray nozzle for additive manufacturing. International Journal of Numerical Methods for Heat & Fluid Flow, 29(7), 2277–2296. https://doi.org/10.1108/hff-10-2018-0553

[16] Srikanth, A., Mohammed Thalib Basha, G., & Venkateshwarlu, B. (2020). A Brief Review on Cold Spray Coating Process. Materials Today: Proceedings, 22, 1390–1397. https://doi.org/10.1016/j.matpr.2020.01.482

[17] Saha, G. C., & Pathak, S. (2020). Cold Spray in the realm of additive manufacturing. Springer.

[18] Badiru, A. B., Valencia, V., V., & Liu, D. (2020). Additive Manufacturing Handbook: Product Development for the Defense Industry (Systems Innovation Book) (1st ed.). CRC Press.

[19] “VRC Metal Systems.” VRC Metal Systems - VRC Metal Systems, 16 June 2021, vrcmetalsystems.com/.

[20] Ashokkumar, M., Thirumalaikumarasamy, D., Thirumal, P., & Barathiraja, R. (2021). Influences of Mechanical, Corrosion, erosion and tribological performance of cold sprayed Coatings A review. Materials Today: Proceedings. https://doi.org/10.1016/j.matpr.2021.01.664

[21] Cold Spray vs Thermal Spray – An Overview - VRC Metal Systems. VRC Metal Systems - VRC Metal Systems. (2021, May 21). https://vrcmetalsystems.com/cold-spray-vs-thermal-spray/.

[22] Cong, D., Li, Z., He, Q., Chen, H., Zhao, Z., Zhang, L., & Wu, H. (2017). Wear behavior of corroded Al-Al_2O_3 composite coatings prepared by cold spray. Surface and Coatings Technology, 326, 247–254. https://doi.org/10.1016/j.surfcoat.2017.07.063

[23] Schmidt, T., Gaertner, F., & Kreye, H. (2006). New developments in cold spray based on higher gas and particle temperatures. Journal of Thermal Spray Technology, 15(4), 488–494. https://doi.org/10.1361/105996306x147144

[24] Max HT series - calefactor de aire by TUTCO SureHeat: Directindustry. El marketplace B2B de la industria. (n.d.). Retrieved February 2, 2022, from https://www.directindustry.es/prod/tutco-sureheat/product-199880-2015583.html

[25] Li, W.-Y., Liao, H., Douchy, G., & Coddet, C. (2007). Optimal design of a cold spray nozzle by numerical analysis of particle velocity and experimental validation with 316L stainless steel powder. Materials & Design, 28(7), 2129–2137. https://doi.org/10.1016/j.matdes.2006.05.016

[26] Chavan, N. M., Vinod Kumar, M., Sudharshan Phani, P., Pant, P., & Sundararajan, G. (2019). Influence of Nozzle Throat Cross Section on Microstructure and Properties of Cold Sprayed Coatings. Journal of Thermal Spray Technology, 28(7), 1718–1729. https://doi.org/10.1007/s11666-019-00913-w

[27] Main. Reym Air. (2021, March 15). https://reymair.com/en/.

[28] EN 1071-6, Advanced Technical Ceramics. Methods of Test for Ceramic Coatings. Determination of the Abrasion Resistance of Coatings by a Micro-Abrasion Wear Test, British Standards Institution, London, UK, 2007, www.bsigroup.com

[29] Chen, J., Ma, B., Liu, G., Song, H., Wu, J., Cui, L., & Zheng, Z. (2017). Wear and corrosion properties of 316L-sic composite coating deposited by cold spray on magnesium alloy. Journal of Thermal Spray Technology, 26(6), 1381–1392. https://doi.org/10.1007/s11666-017-0583-0

[30] He, L., & Hassani, M. (2020). A review of the mechanical and tribological behavior of cold spray metal matrix composites. Journal of Thermal Spray Technology, 29(7), 1565–1608. https://doi.org/10.1007/s11666-020-01091-w

[31] Spencer, K., Fabijanic, D. M., & Zhang, M.-X. (2009). The use of al–al2o3 cold spray coatings to improve the surface properties of magnesium alloys. Surface and Coatings Technology, 204(3), 336–344. https://doi.org/10.1016/j.surfcoat.2009.07.032

[32] Spencer, K., Fabijanic, D. M., & Zhang, M.-X. (2012). The influence of al2o3 reinforcement on the properties of stainless steel cold spray coatings. Surface and Coatings Technology, 206(14), 3275–3282. https://doi.org/10.1016/j.surfcoat.2012.01.031

[33] Li, W., Huang, C., Yu, M., Liu, D., Feng, Y., & Liao, H. (2014). Investigation of high temperature oxidation behavior and tribological performance on cold sprayed nickel–alumina composite coating. Surface and Coatings Technology, 239, 95–101. https://doi.org/10.1016/j.surfcoat.2013.11.024

[34] Osuch-Słomka, E., Ruta, R., and Słomka, Z., "Application of Response Surface Methodology in Ball-Cratering Abrasive Wear Testing," Proc. IMechE Part J: J. Eng. Tribol., Vol. 229, No. 11, 2015, pp. 1379–1392.

[35] Metallographic specimen preparation for 6061 aluminium alloy. (n.d.). Retrieved December 8, 2021, from https://www.metallographic.com/Metallographic-Preparation-Procedures/6061-Aluminum.html.

[36] Rutherford, K. L. and Hutchings, I. M., "A Micro-Abrasive Wear Test, With Particular Application to Coated Systems," Surf. Coat. Technol., Vol. 79, Nos. 1–3, 1996, pp. 231–239.

[37] Rutherford, K. and Hutchings, I. M., "Theory and Application of a Micro-Scale Abrasive Wear Test," J. Test. Eval., Vol. 25, No. 2, 1997, pp. 250–260.

[38] Ortega-Saenz, J. A.; Hernandez-Rodriguez, M. a. L.; Michalczewski, R. Micro-Abrasive Wear Testing of Surface Engineered Surgical Grade CoCrMo Alloy for Biotribological Applications. MPC 2016, 5 (4), 472–484. https://doi.org/10.1520/MPC20160042.

[39] ASTM Standard G99, 2005 (2010), Standard test method for wear testing with a Pin-on-Disc apparatus, ASTM International, West Conshohocken, doi: 10.1520/G0099-05R

APPENDIX

APPENDIX A

Table A.1: State of the Art Equipment

Equipment	Purpose	Results
SEM	Microscope used to observe micro-sized feedstock material, coating surface, coating-substrate adhesion of block samples.	The thickness of the coating was analyzed with this technique.
Microhardness Tester	To perform a Vickers hardness test on the surface of the CSAM coated disk samples.	The microhardness of the CSAM coatings was taken and analyzed.
Calotester	To perform a micro-abrasive calotest on the surface of the disk samples to determine the thickness of the CSAM coating, and the wear rate.	The wear rate of the CSAM coatings was analyzed and data was taken at a different number of revolutions.
Pin-on-Disk	The pin-on-disk will be used to determine the wear rate of the CSAM coatings.	Tribological properties of the nickel based CSAM coatings were taken and analyzed.
Digital microscope Keyence VHX-500F	To characterize and analyze the CSAM coated disk samples.	The morphology and cross sections of the CSAM coating were characterized.

BIOGRAPHICAL SKETCH

Albert Alejandro was born in McAllen, Texas on March 20th, 1999, where he is currently still living. He received education in PSJA (Pharr San Juan Alamo Independent School District) in Pharr, Texas, where he attended Geraldine Palmer Elementary, Liberty Middle School, and was then accepted into the prestigious Thomas Jefferson T-STEM Early College High School which only accepts a select few students every school year. He attended Colorado State University to participate in the NHI Student program in 2014 while he was a sophomore in high school. He then went on to attend STC (South Texas College) after his sophomore year in high school and dedicated all his time and efforts to graduating with an associate degree of science in engineering before finishing high school. He then Graduated from South Texas College in 2017 and went on to graduate high school a week later with a high school diploma and an associate degree in engineering.

He then entered the University of Texas Rio Grande Valley (UTRGV) in Fall 2017 as a junior level student and went on to graduate with a Bachelor of Science in Mechanical Engineering in the spring semester of 2020. After graduating as a mechanical engineer, he began further education by entering the graduate program at UTRGV in Fall 2020. Upon starting his master's degree, he began working at TMAC (Texas Manufacturing Assistance Center) at UTRGV which has allowed him to further continue with research. Albert then graduated from The University of Texas Rio Grande Valley in May 2022 with an MSE in Mechanical Engineering with a focus on additive manufacturing and materials. Albert may be reached by email at albert.al9919@gmail.com